JAERI - M
82-195

STUDIES ON DIVERTOR EFFECTS BY MEANS OF THE DOUBLET- III HIGH-TEMPERATURE PLASMA DEVICE

December 1982

Michiya SHIMADA

日 本 原 子 力 研 究 所
Japan Atomic Energy Research Institute

JAERI-Mレポートは，日本原子力研究所が不定期に公刊している研究報告書です。
入手の問合わせは，日本原子力研究所技術情報部情報資料課（〒319-11茨城県那珂郡東海村）あて，お申しこみください。なお，このほかに財団法人原子力弘済会資料センター（〒319-11 茨城県那珂郡東海村日本原子力研究所内）で複写による実費頒布をおこなっております。

JAERI-M reports are issued irregularly.
Inquiries about availability of the reports should be addressed to Information Section Division of Technical Information, Japan Atomic Energy Research Institute, Tokai-mura, Naka-gun Ibaraki-ken 319-11, Japan.

編集兼発行　日本原子力研究所
印　　刷　(株)原子力資料サービス

JAERI-M 82-195

Studies on Divertor Effects by Means of the Doublet-III High-Temperature Plasma Device

Michiya SHIMADA

Division of Large Tokamak Development
Tokai Research Establishment, JAERI

(Received November 29, 1982)

Divertor actions on impurity removal, helium ash compression and radiative cooling are studied in Doublet-III with an emphasis on the applicability to reacting plasma-grade devices such as INTOR. The following principal results are obtained with a single-null poloidal divertor; no divertor-chamber or divertor-throat exists (referred to as "open divertor geometry") and divertor coils are provided outside the vacuum chamber.

(1) A divertor reduces metallic impurities in the central plasma volume by a factor of 5 -10. A factor of ~ 10 reduction is seen in carbon influx. Oxygen is reduced only modestly, but a factor of two reduction is observed in radiation loss, and a typically peaked radiation power profile is changed to a hollow profile with a divertor.

(2) In helium-seeded divertor discharges, helium gas pressure near the divertor is observed to increase with the increase in the main plasma density. The maximum observed helium pressure is 1×10^{-4} Torr. The helium concentration in the main discharge is deduced to be ~1.6 % from the increase in electron density with a helium gas-puff. This pressure value is high enough to demonstrate the possibility of helium ash exhaust in a diverted tokamak like INTOR with practical-sized pumping ducts.

(3) The radiation power in the divertor volume significantly increases with the increasing plasma density in the main plasma. The maximum observed radiation power is as much as 50 % of the ohmic input power. The radiation power in the main plasma is approximately constant (20 - 30 % of the ohmic input power). This remote radiative cooling reduces the heat load on the divertor plate and the electron temperature near the divertor plate is cooled down to several eV. A significant increase is also observed in the divertor plasma density (higher than 5×10^{13} cm^{-3}). A simple one-dimensional numerical simulation of the radiative divertor elucidates the role of remote radiative cooling in the formation of dense and cold divertor plasma. This remote radiative cooling scheme has the advantage of cooling the divertor plasma without cooling the edge of the main plasma. If this edge cooling scheme can be applied to a diverted tokamak reactor, it may possibly reduce the heat load and the erosion problems of the divertor plates, which are the major drawbacks of a diverted tokamak reactor.

(4) The source of this remote radiative cooling power is experimentally determined to be a mixture of line radiation of hydrogen neutral and oxygen. A simple model calculation of impurity line radiation in the divertor shows the feasibility of remote radiative cooling in INTOR.

In light of obtaining these useful results, the installation of a divertor in reacting-plasma-grade fusion devices appears to be very effective for sustaining the long-lived operational conditions of a reacting plasma.

Keywords: Fusion Reactor, Divertor, Impurity Reduction, Ash Exaust

---

This work was performed under a cooperative agreement between the Japan Atomic Energy Research Institute and the United States Department of Energy under DOE Contract No. DE-AT03-80SF11512.

JAERI－M 82－195

ダブレットⅢ高温プラズマ装置による ダイバータ効果の研究

日本原子力研究所東海研究所大型トカマク開発部
嶋田　道也

（ 1982 年11月29日受理 ）

ジュール加熱期のダイバータ効果の研究の総合報告である。

1）ダブレットⅢのダイバータはダイバータスロートなし，ダイバータ室なし，及びダイバータ・コイルが真空容器の外置きという従来のダイバータ付トカマクにない特徴をもっている。この形状のダイバータによって，不純物除去・灰排気という核融合炉には不可欠の特性が実験的に証明された。

2）ダブレットⅢのダイバータでは，主プラズマの密度を増加させるとダイバータ部の放射冷却が強くなり，それによるダイバータ板の熱負荷軽減，ダイバータ・プラズマの温度低下が起こる。この効果により核融合炉のダイバータ板の寿命が著しく長くでき，保守が容易になる可能性がある。

Contents

目　　次

1. Introduction

1.1 Motivation and Objectives of Divertor Research in Doublet-III

Poloidal divertors are considered to be the most reliable means of impurity removal and helium ash exhaust, both of which are crucial issues for thermonuclear fusion research. The pioneering research of the DIVA group [1] demonstrated the impurity removal capability of a poloidal divertor. All divertor studies so far have concentrated on a closed divertor geometry (i.e., a divertor with a divertor chamber and divertor throat), and the divertor coils have been located inside the vacuum chamber. However, these two features are not feasible for fusion reactors due to the concurrent mechanical complexities of the divertor structure.

The single-null poloidal divertor in Doublet-III has two unique features: i) an open divertor geometry (no divertor chamber or divertor throat), and ii) divertor coils located outside the vacuum chamber; both of these are very attractive from the viewpoint of reactor design, due to their simple structure. The INTOR*note) design group employs an open divertor geometry with the divertor coils situated outside the vacuum chamber [2]. Therefore, it is both important and urgent to investigate the divertor capabilities demonstrated by this simple divertor, and provide a physics design basis for fusion reactors employing divertors.

---

*note) The INTOR is a next-stage, large-scale Tokamak-type experimental reactor being proposed by the IAEA-International Design Team, in which Japan, the U.S.A., the European Communicty (EC) and the U.S.S.R. are participating.

No experimental effort has been made to test the helium ash exhaust capability of divertors, although helium ash exhaust is a crucial issue in maintaining a steady-state fusion reactor. Helium ash particles, unless steadily exhausted, dilute the fuel and degrade fusion reactivity, since fusion reactors will be operated with β values in close proximity to the maximum available β. The single-null poloidal divertor in Doublet-III has successfully demonstrated a strong capability to exhaust helium ash [3,4].

Had the heat load and erosion problems of the divertor plate not been solved, a poloidal divertor would have been much less attractive. The single-null poloidal divertor in Doublet-III has manifested a promising capability for remote radiative cooling [3,5,6]. The divertor plasma radiates away the high heat flux (80 MW, or 200 W/cm^2 in INTOR) transported from the hot core before it reaches the divertor plate, thus protecting the divertor plate. Risky operation with a high heat flux (200 W/cm^2, which is the engineering limit of the steady-state heat removal rate) onto the divertor plates can be avoided by the remote radiative cooling capability of the divertor plasma. Radiative cooling of the divertor plasma also results in a reduction of divertor plate erosion which improves the reliability, maintainability, and longevity of a fusion reactor.

1.2 Impurity Problems in Tokamaks

Impurities, or non-hydrogenic atoms in plasmas, have long been recognized as one of the major problems for experimental plasma physicists. The most illustrative experiments of the impurity effect on a tokamak discharge were reported by the PLT group [7, 8]. The discharges with tungsten or stainless-steel limiters were characterized by centrally peaked radiation loss, poor confinement, and therefore poor heating efficiency. In order to reduce metallic impurities, a water-cooled graphite limiter proved to be essential for high power heating experiments.

Impurities are divided into two categories. One is light (or low-Z) impurities such as carbon or oxygen. The other is metallic (or high-Z) impurities such as titanium, chromium, iron, nickel, tungsten, or molybdenum which are major components of the first wall and the limiter. The light impurities are relatively well-behaved. The calculation by Post and Jensen [9] shows that the radiative cooling rate of low-Z elements have peaks in the low temperature range (less than 100 eV), whereas the high-Z elements have peaks in the higher temperature range. Therefore, the low-Z elements radiate at the plasma edge, and the high-Z elements radiate near the center. Moreover, the peak radiative cooling rate for high-Z impurities is typically two orders of magnitudes higher than that for low-Z impurities.

The methods for reducing light impurities have been well explored. Stott [10] first used titanium gettering to reduce light impurities and produced plasmas with Z_{eff} near one. Taylor [11] is credited with inventing the low-temperature discharge cleaning method. Both of these have become conventional techniques for cleaning the first wall.

No practical methods for controlling metallic impurities were known until the pioneering works on poloidal divertors by the DIVA group [1]. The mechanisms for metallic impurity production which were investigated by this group [12] were 1) ion-sputtering, 2) arcing, and 3) evaporation. Ion-sputtering proved to be the major impurity generating mechanism during stable discharges; arcing produces impurities during unstable discharge stages such as disruption and breakdown; evaporation is a minor mechanism in small devices except for runaway electrons, but becomes important in high power, long-pulse devices. The ion-sputtering yield reviewed by MacCracken [13] is a strongly increasing function of electron temperature. It is widely recognized that electron temperature has to be kept below 50 eV in front of the first wall or the divertor plate so as to avoid serious sputtering and high erosion problems [14]. In order to reduce evaporation, heat flux must be distributed throughout a large area. Locally concentrated heat loads should be avoided as much as possible.

The DIVA group showed that metallic impurities can be reduced by a poloidal divertor. The advantages of a poloidal divertor or magnetic limiter are:

1) to establish a plasma-vacuum interface without using a material limiter, thus hindering the intrusion of limiter materials into the plasma,

2) to localize plasma-wall interaction away from the main discharge, and furthur reduce the impurity influx by friction force with the plasma flow,

3) to guide the plasma flow to the divertor plate so that impurities can be shielded in the scrape-off layer.

However, these characteristics can also be a disadvantage in future reactors with divertors such as INTOR [2] due to :

a) concentrated heat load to the divertor plates.
   (about 200 W/cm^2 for INTOR)
b) high erosion rate of the divertor plate due to high particle flux with electron temperatures of 100-400 eV.
   (about 25 cm/yr for INTOR)

Therefore, unless the following two problems are solved, divertors will not be feasible for reactors:

A) reduction of the heat load to the divertor plates (less than 50 W/cm^2),
B) reduction of the electron temperature near the divertor plate to less than 50 eV, hopefully to below 10 eV.

1.3 Helium Ash Exhaust in Tokamaks

Helium particles are unavoidably produced by a D-T fusion reaction. Therefore, a reliable means of compressing the helium ash near the pump duct should be investigated. The experiments by Overskei [15] suggest that the pumped-limiter scheme might work. His idea is to utilize the fact that most of the particle recycling (about 80 %) is concentrated at the limiter [16]. (His measurements of working gas pressures behind the limiter have been as high as 20 mTorr.) The PDX [17], ISX [18] and MACROTOR [19] groups have also recently observed equally high pressures behind the limiter. This approach is very attractive from the viewpoint of both 1) low cost, and 2) simple design. High heat load on the leading edge, however, makes the feasibility for a fusion reactor questionable.

Helium ash exhaust by use of a poloidal divertor was proposed by Shimomura and Seki [20, 21]. Their calculations show that helium partial pressure will be 1×10^{-5} Torr near the divertor plate. As the alpha-particle generation rate is 5 Torr ℓ/sec in INTOR, the required pumping speed will be 5×10^{5} ℓ/s, which is a marginal engineering possibility. Helium enrichment is another interesting aspect from the viewpoint of tritium inventory (see §5.1). They also showed that helium ash is weakly enriched by the divertor (20 %) because of the larger charge-exchange rate for hydrogen so that fuel particles flow back to the main discharge more easily than helium particles. Recent calculations by the Princeton group [22], however, indicate that there will be no enrichment in the divertor. A scheme for enriching helium was recently proposed by Sugihara and Abe [23]. Their idea is to replace one row of blankets by a "Palladium Alloy Membrane" which allows fuel particles to flow back to the main plasma. Their calculations show that a factor of five enrichment can be achieved by this approach.

Although helium ash exhaust is widely recognized as one of the major problems of thermonuclear fusion research there is no experimental work that addresses the following problems:

A) the measurement of helium partial pressure with hydrogen discharges and proof that it may reach above 1×10^{-5} Torr, and

B) the measurement of helium concentration in discharges to determine whether helium enrichment is occurring or not.

1.4 Review of Divertor Studies in Doublet-III and Scope of This Thesis

The successful operation of the Doublet III single-null poloidal divertor demonstrates some new advantages for a diverted tokamak in addition to the impurity influx suppression capability demonstrated in DIVA. The new advantages are ;

1) impurity reduction with an open geometry [3,5,24,25]
2) remote radiative cooling [3,5]
3) helium ash compression capability [3,4]

A natural single-null divertor configuration, which is obtained as a simple modification of the D-shaped plasma cross sections in Doublet-III, illustrates an impurity reduction capability without a divertor chamber and with the divertor coils outside the vacuum chamber [24]. In diverted discharges, a significant, non-linear increase is observed in the plasma density and particle recycling in the divertor with the increase of the main plasma density [25]. This results in a large radiation power density in the divertor region [3,5] and a large increase in the helium pressure in the divertor region [3,4]. High helium pressure in the divertor will facilitate helium ash exhaust in future fusion reactors. Strong remote radiative cooling will possibly negate the heat load and erosion problems of the divertor plate, which are the major drawbacks of diverted tokamaks. Moreover, remote radiative cooling by a divertor provides an edge cooling and heat removal scheme for fusion reactors.

This work presents the experimental results of helium compression and remote radiative cooling in the divertor using the single-null poloidal divertor in Doublet-III, with an emphasis on the applicability to INTOR-grade devices. In Chapter 2, the Doublet-III device and its diagnostics are described. Chapter 3 discusses the formation of the divertor equilibrium and summarizes new experimental results. In Chapter 4, experimental results on impurity reduction and localized particle accumulation and recycling in the divertor are presented. Helium ash exhaust experiments are described in Chapter 5. Chapter 6 deals with remote radiative cooling in Doublet-III and also discusses the feasibility of a remote radiation cooling scheme in INTOR. The conclusions are summarized in Chapter 7, where the subjects for future investigation are also presented.

REFERENCES (Chapter 1)

[1] DIVA GROUP, Nucl. Fusion 18 (1978) 1619.

[2] INTOR group, "International Tokamak Reactor - Phase One" IAEA, Vienna (1981) to be published.

[3] SHIMADA, M., IOKI, K., NAGAMI, M., YOKOMIZO, H., IZUMI, S., et al., in Controlled Fusion and Plasma Physics (Proc. 10th Europ. Conf. Moscow, 1981) Vol. 1 (1981) J1.

[4] SHIMADA, M., NAGAMI, M., IOKI, K., IZUMI, S., MAENO, M., et al., Phys. Rev. Lett. 47 (1981) 796.

[5] SHIMADA, M., NAGAMI, M., IOKI, K., IZUMI, S., MAENO, M., et al., Nucl. Fusion 22 (1982) 643.

[6] SHIMADA, M., NAGAMI, M., IOKI, K., IZUMI, S., MAENO, M., et al., "High Density, Single-Null Poloidal Divertor Results in Doublet III", to be published in J. of Nucl. Mat. (Chapter 4, 5, 6).

[7] BOL, K., ARUNASALAM, V., BITTER, M., BOYD, D., BRAU, K., et al., in Plasma Physics and Controlled Nuclear Fusion Research (Proc. 7th Int. Conf. Innsbruck, 1978)) Vol. 1, IAEA, Vienna (1979) 11.

[8] EUBANK, H., GOLDSTON, R. J., ARUNASALAM, V., BITTER, M., BOL, K., et al. in Plasma Physics and Controlled Nuclear Fusion Research (Proc. 7th Int. Conf. Innsbruck, 1978)) Vol. 1, IAEA, Vienna (1979) 167.

[9] POST, D. E., JENSEN, R. V., TARTER, C. B., GRASBERGER, W. H., and LOKKE, W. A., Atomic Data and Nuclear Data Tables 20 (1977) 397.

[10] STOTT, P. E., DAUGHNEY, C. C., ELLIS, R. A., Nucl. Fusion 15 (1975) 431.

[11] OREN, L., TAYLOR, R. J., Nucl. Fusion 17 (1977) 1143.

[12] OHASA, K., MAEDA, H., YAMAMOTO, S., NAGAMI, M., OHTSUKA, H., et al., Nucl. Fusion 18 (1978) 872.

[13] McCRACKEN, G. M., and STOTT, P. E., Nucl. Fusion 19 (1979) 889.

[14] SHIMOMURA, Y., Nucl. Fusion 17 (1977) 626.

[15] OVERSKEI, D., Phys. Rev. Lett. 46, 177 (1981).

[16] UEHARA, K., GOMAY, Y., YAMAMOTO, T., SUZUKI, N., MAENO, M., et al., Plasma Phys. 21 89 (1979).

[17] JACOBSEN, R., and BUDNY, R., Bulletin of the American Physical Society 26 (1981) 1059.

[18] EDMONDS, P. H., MADISON, J. M., and MIODUSZEUSKI, P. K., Bulletin of the American Physical Society 26 (1981) 880.

[19] TALMADGE, S., and TAYLOR, R., Bulletin of the American Physical Society 26 (1981) 1059.

[20] SHIMOMURA, Y. SAKO, K., SHINYA, K., "Some Considerations of Ash Enrichment and Ash Exhaust by a Simple Divertor", Japan Atomic Energy Research Institute Report No. JAERI-M8294 (1979).

[21] SEKI, Y., SHIMOMURA, Y., MAKI, K., AZUMI, M., TAKIZUKA, T., Nucl. Fusion 20, 1213 (1980).

[22] CALLEN, J. D., EMMERT, G. A., BAILEY, A. M., BENCHIKH-LEHOCINE, M. E., DAVIDSON, J. N., et al., in Plasma Physics and Controlled Nuclear Fusion Research (Proc. 8th Int. Conf. Brussels, 1980) Vol. 2, IAEA, Vienna (1981) 775.

[23] SUGIHARA, M., and ABE, T., Nucl. Fusion 21 (1981) 1024.

[24] NAGAMI, M., SHIMADA, M., YOKOMIZO, H., SEKI, S., KONOSHIMA, S., et al., Nucl. Fusion 18 (1980) 1325.

[25] NAGAMI, M., FUJISAWA, N., IOKI, K., KITSUNEZAKI, A., KONOSHIMA, S., et al., in Plasma Physics and Controlled Nuclear Fusion Research (Proc. 8th Int. Conf. Brussels, 1980) Vol. 2, IAEA, Vienna (1981) 367.

2. General Description of Doublet-III Device

2.1 Doublet-III device

Doublet-III is a large-size tokamak device with a vertically elongated vacuum vessel [1]. Figure 1 shows the cross-section of the device. The machine and the plasma parameters are summarized as follows ;

plasma major radius	143 cm
plasma horizontal width	90 cm
height of the vacuum vessel	270 cm
vacuum vessel back-up limiters and divertor plates	Inconel
primary limiter	TiC-coated graphite (water-cooled)
maximum toroidal field	24 kG
maximum plasma current	1 MA
discharge duration	1 sec
ohmic heating power	0.5 - 1 MW.

The divertor plates are half-cylindrical shaped, 6 cm in width, 13 cm in height. They are installed in vertical rows, 26 cm apart in toroidal direction, 90 cm in total vertical height.

By controlling the poloidal flux values on the 24 poloidal field coils, either circular or non-circular equilibria including divertor can be produced [2, 3, 4]. Experiments described in this work are performed with ohmically-heated hydrogen discharges, toroidal field of 24 kG, plasma current of 300-500 kA, line-average electron density of $(1.5 - 5)\times10^{13}$ cm^{-3}. The central electron temperature is 0.6 -1.4 keV, Z_{eff} is 1.1 -2.0.

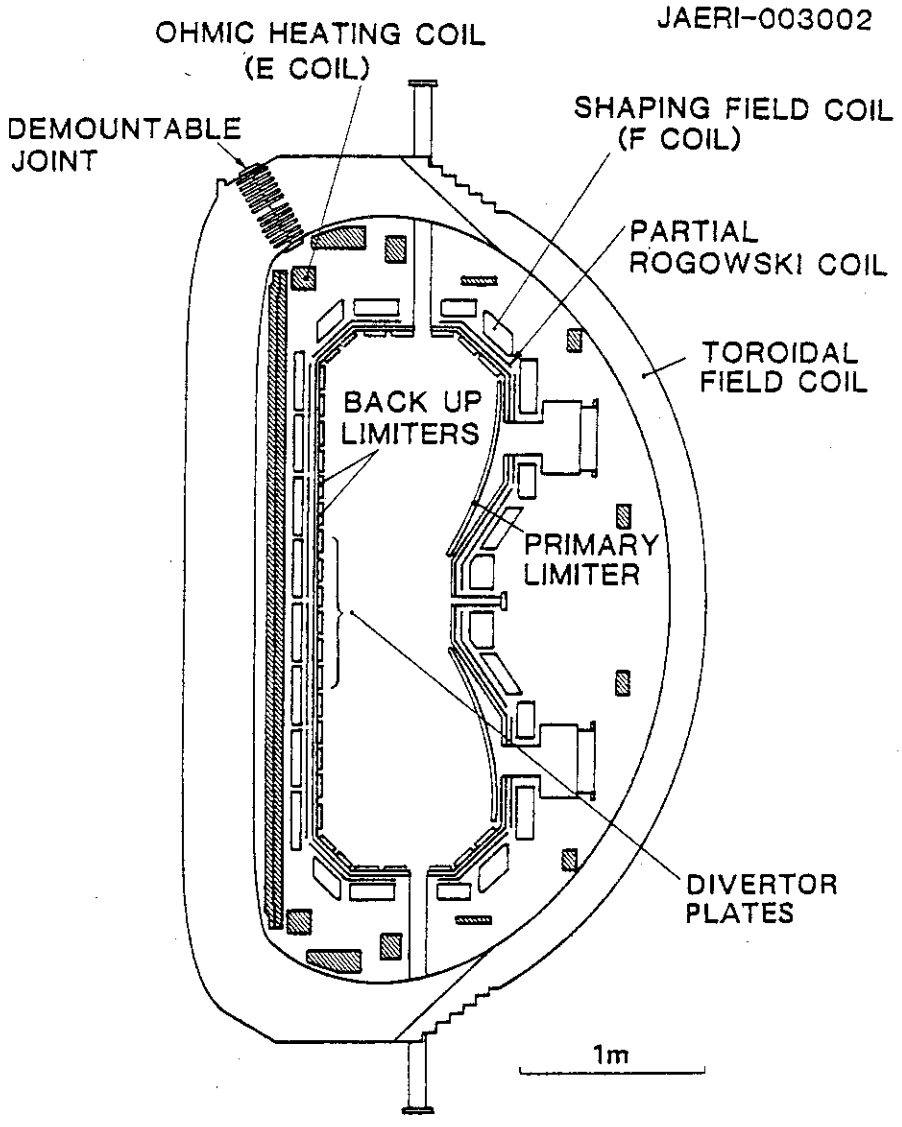

FIG. 2.1 Cross-sectional view of the Doublet-III device. Axisymmetric axis is on the left. Plasma major radius is 143 cm, plasma horizontal minor radius is 45 cm, height of the vacuum vessel is 270 cm. Shown in the figure are : Toroidal coil (maximum field : 24 kG, 26 coils), ohmic heating coils (ohmic-heating flux swing : 5.0 V·sec), shaping field coils (24 coils), vacuum vessel (Inconel, double-layer), primary limiter (water-cooled TiC-coated graphite), and back-up limiters (Inconel), and backup limiters indicated in the figure are utilized as divertor-plates.

2.2 Diagnostics

Figure 2.2 shows all the diagnostics on the Doublet-III device.

The major diagnostic equipments are summarized as follows ;

magnetics
- poloidal flux loops (24 loops)
- partial rogowski coils, magnetic probes

electron density
- 2 mm microwave interferometer*
- CO_2 vertical interferometer
- CO_2 tangential interferometer array (profile)

electron temperature
- 90° Ruby-laser Thomson scattering
- $2\omega_{ce}$ radiometer (profile)
- Soft-X ray energy analyzer (profile)

spectroscopy
- vuv monochromator (15 - 650 Å)
- photodiodes array*(O I, O II, C III, H_α, He I, He II)
- visible TV*(tangential)

power balance
- 21 channel and 5 channel bolometer array*
- IR camera*(primary limiter, divertor plates)
- thermocouples*(primary limiter, divertor plates, back-up limiters)

neutral pressure
- ionization gauges*
- capacitive manometer
- quadrupole mass analyzer*

magnetohydrodynamic activity, Z_{eff}
- PIN diodes array (vertical, and tangential)

The symbol (*) denotes diagnostics available for divertor measurements.

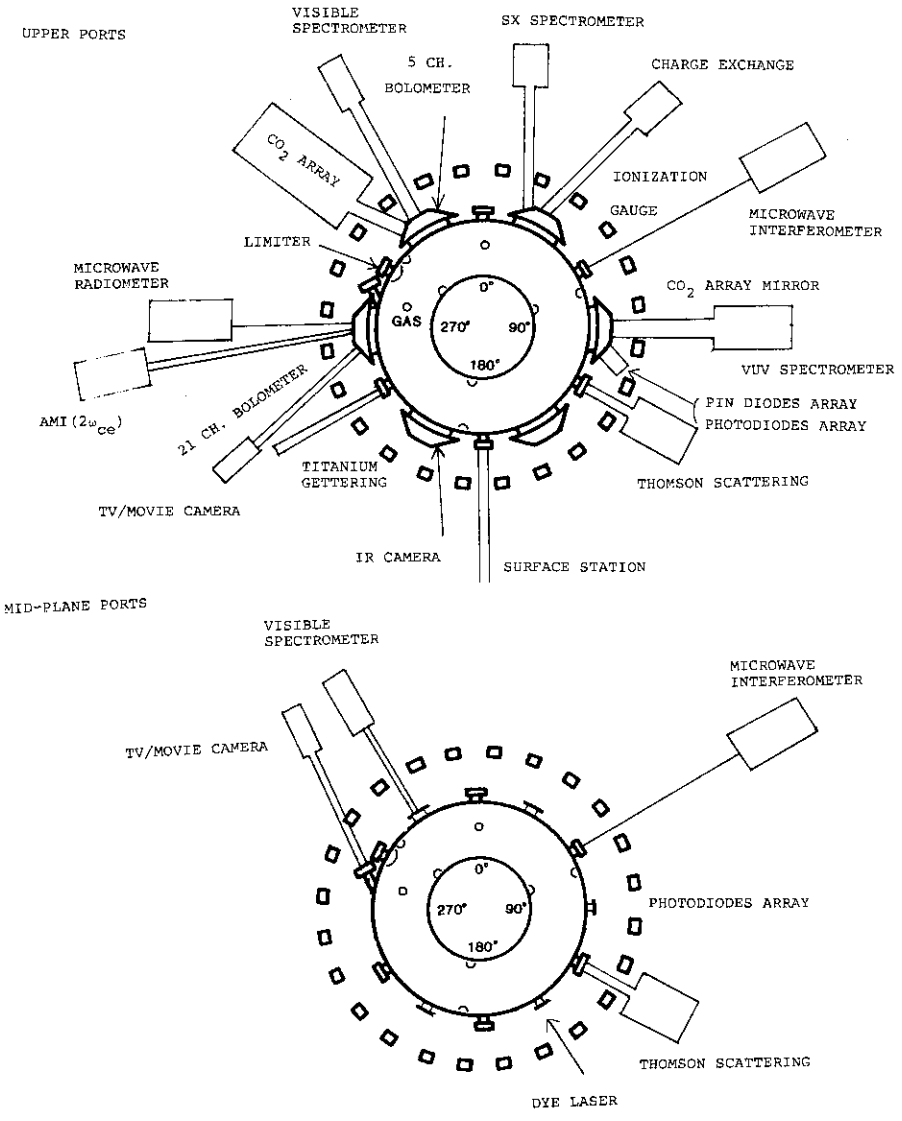

FIG. 2.2

Diagnostic arrangements for Doublet-III

REFERENCES (Chapter 2)

[1] CALLIS, R. W., Doublet-III Baseline Design Description, General Atomic Company Report GA-A13996 (1976).

[2] JAERI TEAM, Nucl. Fusion 20 (1980) 1455.

[3] YOKOMIZO, Y., NAGAMI, M., SHIMADA, M., BROOKS, N., SERAYDARIAN, R., et al., Japan Atomic Energy Research Institute Report JAERI-M9698 (1981).

[4] YOKOMIZO, H., NAGAMI, M., SHIMADA, M., YOSHIDA, H., MAENO, M., et al., in Controlled Fusion and Plasma Physics (Proc. 10th Europ. Conf. Moscow, 1981) Vol. 1 (1981) A7.

3. Equilibrium of Divertor Configuration and Overview of New Experimental Results

3.1 Divertor Equilibrium [1, 2]

The single-null poloidal divertor equilibria is obtained with a simple modification of the D-shaped plasma. Figure 3.1 shows the formation of single-null divertor equilibria. Shown in the figure are three cases of the cross section of the magnetic surface (flux plots) corresponding to the three actual experimental conditions which have been obtained from an MHD calculation. The separatrix magnetic surface appears inside the vacuum vessel when I_D/I_p exceeds 0.35. I_p is the plasma current and I_D is the divertor current defined as the sum of currents through the particular shaping coils, 1A and 1B. For I_D/I_p = 0.58, the main plasma is separated from the limiters and walls by more than 7cm (the ratio of the vertical size to the horizontal width of the plasma cross section of 1.32). These equilibria are confirmed by a tangential TV observation of plasma cross sections which can identify the two-dimensional plasma-limiter interaction by observing the distribution of the intensity of visible light (4000 Å ~ 8000 Å) in the plasma periphery.

Figure 3.2 shows the TV observations in the discharges corresponding to Fig. 3.1. The inside view of the vacuum chamber is also shown. In the non-diverted discharges, the TV shows that the plasma interacts intensively with the inside, outside and top limiters. In the marginally diverted discharges of I_D/I_p = 0.35, plasma-limiter interaction is decreased, particularly on the inside limiter and strong light emission appears on the inside wall near the mid-plane of the vacuum chamber. At I_D/I_p = 0.58, the plasma limiter interaction at the main plasma periphery decreases significantly, and intense light emission appears on the inside wall where the separatrix magnetic surface intersects the wall.

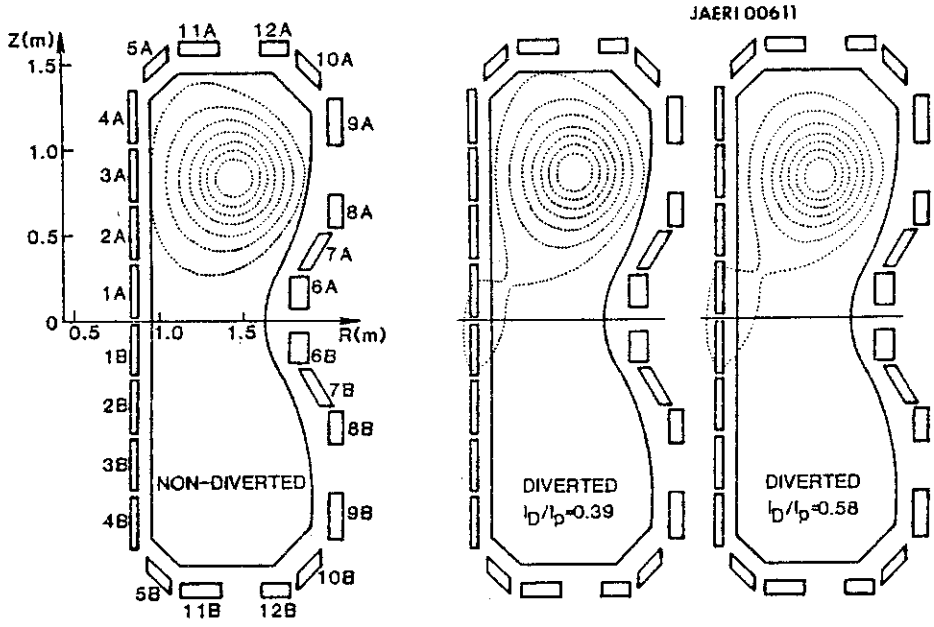

FIG. 3.1 Three cases of the cross-section of magnetic surfaces from an MHD equilibrium calculation from three experimentally obtained configurations, with different divertor currents I_D. Two coils (1A, 1B) are employed as divertor coils.

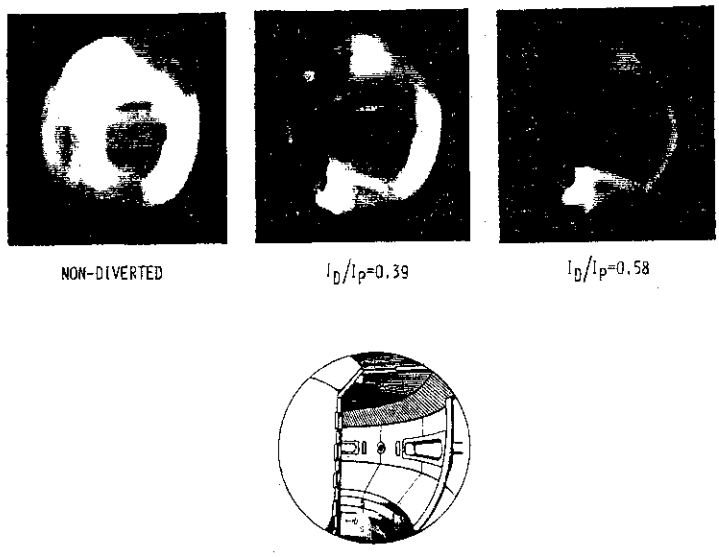

FIG. 3.2 Tangential TV pictures (ranges of wavelength covered are 4000 -8000 Å) for three different configurations in FIG. 1. The field of view (see inset figure) includes the primary limiter (on the right), top limiters, and iside back-up limiters (left) and divertor plates (left below). The intersection point of the separatrix flux surface (Ψ_s) with the wall is indicated.

3.2 Overview of New Experimental Results

New experimental results to be presented in this dissertation are summarized as follows ;

1) impurity reduction implemented by open divertor geometry.
2) non-linear increase of divertor electron density and recycling.
3) strong radiative cooling in the divertor up to 50 % of joule input power.
4) formation of dense and cool divertor plasma ($n_e \geq 5 \times 10^{13} cm^{-3}$, $T_e \leq 7$ eV).
5) high pressure of hydrogen and helium near the divertor (P_{H_2} up to 4×10^{-3} Torr, P_{He} up to 1×10^{-4} Torr).
6) weak helium de-enrichment.

REFERENCES (Chapter 3)

[1] NAGAMI, M., SHIMADA, M., YOKOMIZO, H., SEKI, S., KONOSHIMA, S., et al., Nucl. Fusion 18 (1980) 1325.

[2] NAGAMI, M., FUJISAWA, N., IOKI, K., KITSUNEZAKI, A., KONOSHIMA, S., et al., in Plasma Physics and Controlled Nuclear Fusion Research (Proc. 8th Int. Conf. Brussels, 1980) Vol. 2, IAEA, Vienna (1981) 367.

4. Reduction of Impurities, Accumulation of Particles and Particle Recycling by Divertor

4.1 Reduction of Impurity by Divertor

Reductions of the influx and concentration of metallic impurities by the divertor are observed as shown in Fig. 4.1, where Ni XXI 95.9Å and Ni XI 148.4Å (both $\Delta n = 0$ transitions; n is the principal quantum number) line emissivities along the radial chord of the main plasma are compared for similar discharges with and without the divertor. Ni XI line emission is proportional to the intensity of the nickel influx into the main plasma. Ni XXI intensity divided by electron density is a measure of the concentration of nickel in the plasma center, for constant electron temperature. Since the electron temperature difference between these diverted and non-diverted discharges is found to be relatively minor (~10%), fall in Ni XXI line intensity may be attributed primarily to the reduction in nickel density. In diverted discharges, the concentration of nickel is reduced by a factor of 5 -10 compared with that of well-tuned non-diverted discharges (n_{Ni}/n_e is $\sim 10^{-3}$ in low density non-diverted discharges, and $\sim 10^{-5}$ for high density non-diverted discharges).

The carbon influx is also dramatically suppressed by the divertor. The density dependence of the C IV line (1548Å) is shown in Fig. 4.2 with and without divertor. Divertor operation reduces the carbon influx by as much as a factor of 10.

Oxygen is moderately reduced by the divertor. Fig. 4.3 is the O VII 21.6Å line intensity with and without the divertor, indicating an oxygen reduction by a factor of two in the low density region and no reduction in high density. This is in agreement with the ASDEX result [1]. Figure 4.4 shows the comparison of the radiative power loss, P_r, in the main plasma for diverted and non-diverted discharges with a plasma current of 500kA and a toroidal field of 24kG as a function of line-averaged electron density. The radiation loss in the main plasma is reduced by a factor of 2 with the divertor operation as a result of the impurity reduction implemented by this "open divertor" geometry (or without divertor chamber). The typically peaked radiation profile with a non-diverted discharge changes into a hollow profile with the divertor (Fig. 4.5). This phenomenon is consistent with the reduction of metellic impurities by the divertor (Fig. 4.1).

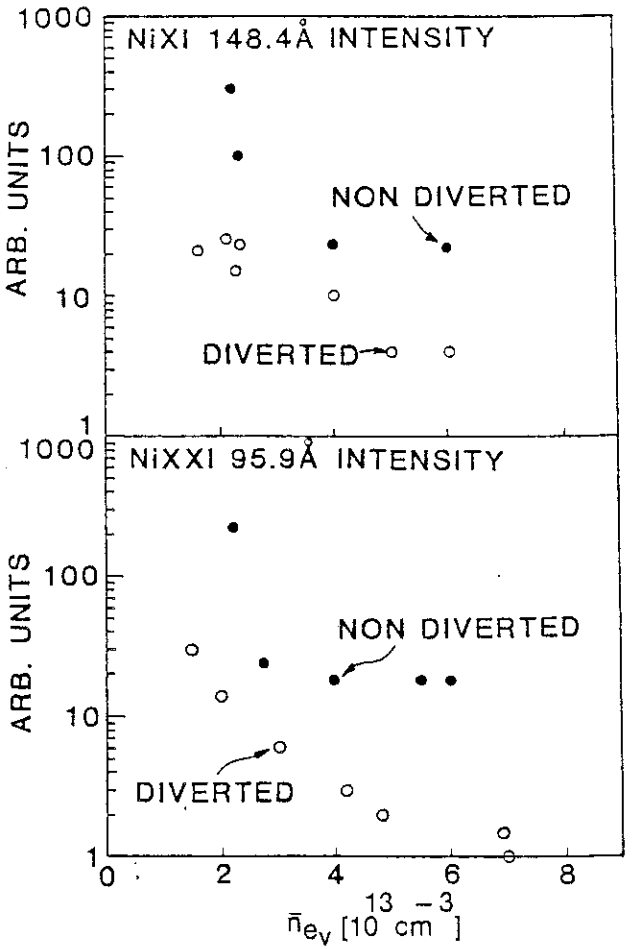

FIG. 4.1 The line intensities of Ni XI, Ni XXI as a function of $\bar{n}_e$ (line-averaged electron density of the main plasma) with and without the divertor. The divertor reduces the influx and concentration of metallic impurity by a factor of 5-10.

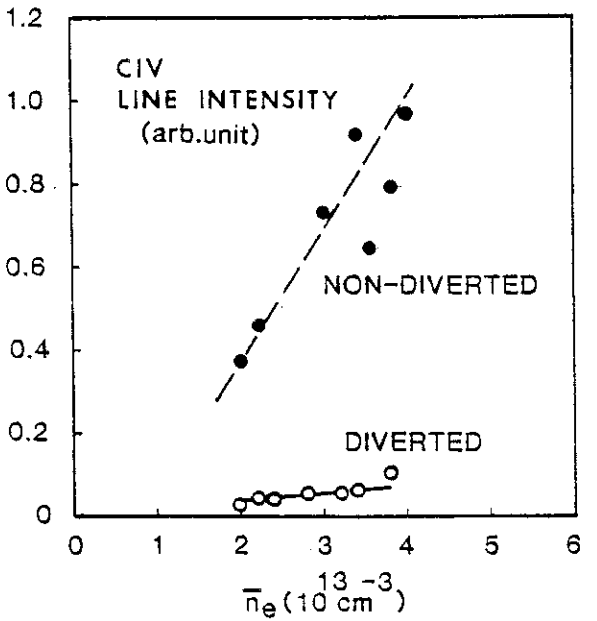

FIG. 4.2 C IV line intensity as a function of $\bar{n}_e$ with and without the divertor. Carbon impurity influx is reduced by a factor of 10 by the divertor.

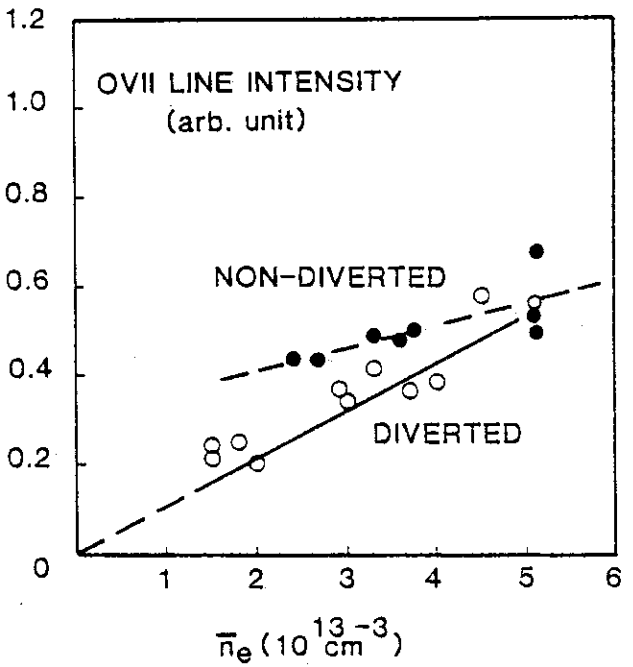

FIG. 4.3 O VII line intensity 21.6Å as a function of $\bar{n}_e$ (line-averaged electron density of the main plasma) with and without the divertor. Oxygen is moderately reduced by the divertor.

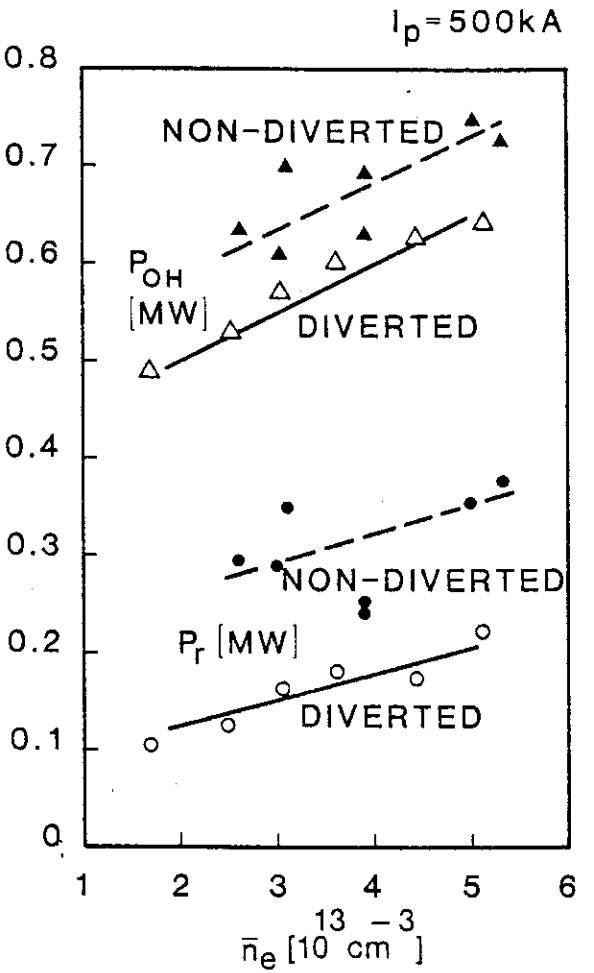

FIG. 4.4 The radiation power P_r in the main plasma, and ohmic input power P_{OH} as a function of $\bar{n}_e$. The divertor reduces the radiation loss in the main plasma P_r by a factor of ~ 2.

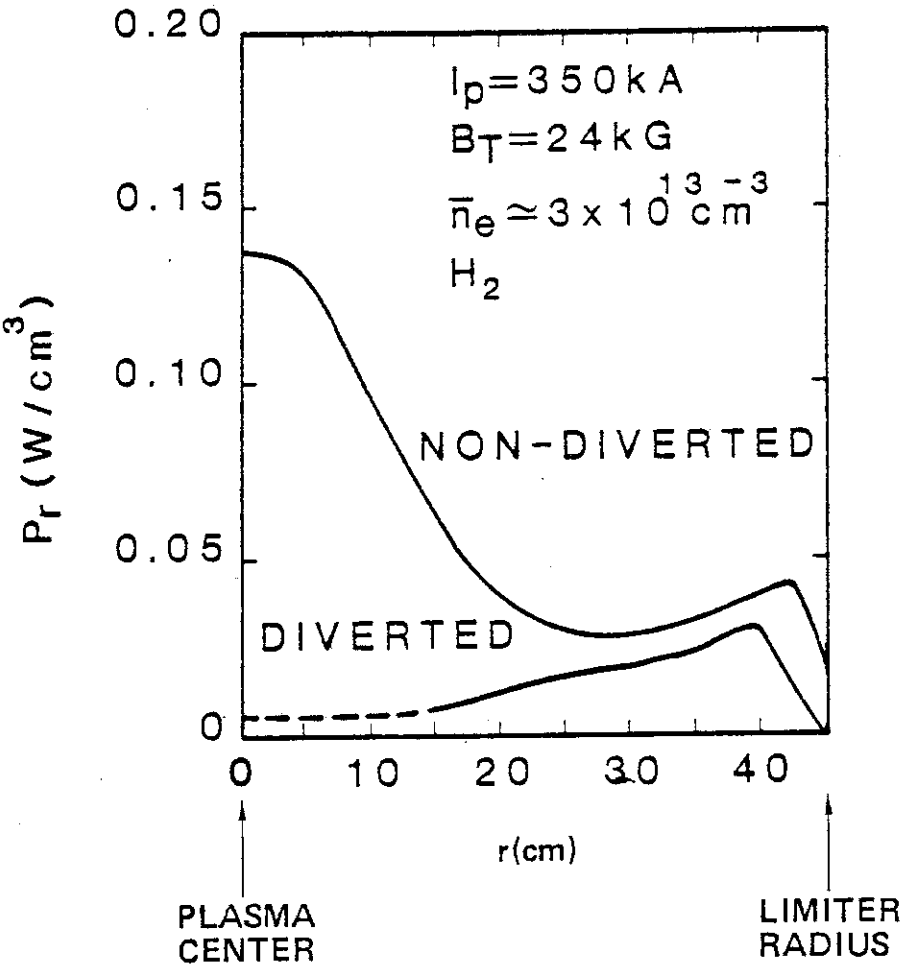

FIG. 4.5 The radiation power density profiles $P_r(r)$ for discharges with and without the divertor.

4.2 Accumulation of Particles and Particle Recycling at Divertor

Figure 4.6 shows the line-averaged electron density measured along a horizontal path ($\bar{n}_{e_{DIV}}$) at the divertor region (the path-length ℓ = 67 cm) as a function of the line-averaged electron density of the main plasma measured along a horizontal path ($\bar{n}_e$). Also shown are the H_α line-emissions from the main plasma and the divertor as a function of $\bar{n}_e$. From this figure, one sees that $\bar{n}_{e_{DIV}}$ and $H_{\alpha_{DIV}}$ increase non-linearly with $\bar{n}_e$. The separatrix field line deduced from an MHD equilibrium calculation and the TV observed O I and H_α peak line emissions are located ~ 10 cm apart from the inside wall. With these factors taken into account, the non-linear increments of $\bar{n}_{e_{DIV}}$ and $H_{\alpha_{DIV}}$ occur within the horizontal width of ~ 10 -30 cm. With this width, the actual $\bar{n}_{e_{DIV}}$ is a factor of ~ 2 -7 larger than that deduced with ℓ = 67 cm. Therefore, the electron density in the divertor region appears to be higher than 5 x 10^{13} cm^{-3}.

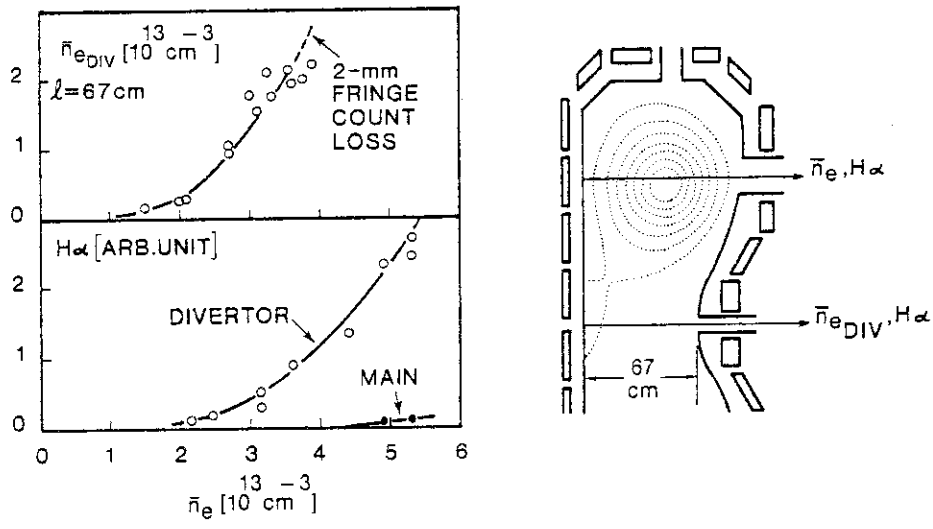

FIG. 4.6 The line-averaged electron density of the divertor (ℓ = 67 cm) $\bar{n}_{e_{DIV}}$ as a function of $\bar{n}_e$ (line-averaged electron density of the main plasma). H_α line intensity measured along the central chord, and the chord through the divertor vs. $\bar{n}_e$. Both $\bar{n}_{e_{DIV}}$ and $H_{\alpha_{DIV}}$ show a significant, non-linear increase with increasing $\bar{n}_e$.

The n_e-value at the divertor region may be locally higher than 5 x 10^{13} cm^{-3} because the measurement with a 2 mm microwave (with a cut-off density of 2.5 x 10^{14} cm^{-3}) has a beam refraction problem when $\overline{n}_{eDIV}$ (ℓ = 67 cm) is more than ~ 2 x 10^{13} cm^{-3}. The particle confinement time in the divertor region, deduced from H_α line intensity and ionization rate [2], is ~ 1 msec. This value shows reasonable agreement with the lifetime of protons evaluated as lost to the divertor wall with the flow velocity along the scrape-off field lines of 0.3 Cs [3] (where Cs denotes the ion acoustic speed and T_e is assumed to be ~ 7 eV).

The strong accumulation of particles and recycling in the divertor region during high density operation is consistent with radiative cooling of the divertor plasma, which will be discussed in Chapter 6. And, they are also consistent with a reduction of the attenuation length (λ) of neutral hydrogen particles produced at the wall with the increase of plasma density in the divertor region: λ ~ 10 cm at n_e = 1 x 10^{13} cm^{-3} and λ < 3 cm at $n_e \geq$ 5 x 10^{13} cm^{-3}, both with T_e ~ several eV. This phenomenon observed in Doublet III, which is a relatively large device (the plasma radius a ~ 40 cm), is significantly different from that observed in a small device, such as DIVA (a ~ 10 cm), where a linear relation of $\overline{n}_e$ and $\overline{n}_{eDIV}$ was observed. This provides new advantages for employing a divertor in future large tokamaks. These advantages will be further discussed in the following sections.

4.3 Summary of Chapter 4

In this chapter, the experimental results on impurity reduction, and high-density divertor plasma have been presented. The main conclusions are summarized as follows:

1) Impurities and the radiation loss of the main plasma are reduced with an open divertor geometry.

2) A non-linear increase of the electron density and particle recycling at the divertor is observed with increasing electron density of the main plasma.

3) The electron density in the divertor region may attain a value in excess of 5×10^{13} cm^{-3} in high-density divertor operation.

REFERENCES (Chapter 4)

[1] KEILHACKER, M., ALBERT, D. B., BEHRINGER, K., BEHRISCH, R., ENGELHARDT, W., et al., in Plasma Physics and Controlled Nuclear Fusion Research (Proc. 8th Int. Conf. Brussels, 1980) Vol. 2, IAEA, Vienna (1981) 351.

[2] JOHNSON, L. C., HINNOV, E., J. Quant. Spectrosc. Radiat. Transfer 13 (1979) 333.

[3] SHIMOMURA, Y., MAEDA, H., J. Nucl. Mater. 76 & 77 (1978) 617.

5. Helium Ash Exhaust by Divertor

5.1 Helium Ash Exhaust

Helium ash exhaust is one of the most important issues in thermonuclear fusion research. The alpha particles will, unless exhausted, dilute the fuel particles and deteriorate fusion reactivity since total particle density is limited by the maximum allowable β. A simple divertor was proposed for the INTOR tokamak by Shimomura, et al. [1, 2, 3]. Their calculation showed the helium pressure at the divertor plate to be 1×10^{-5} Torr. The pumping speed then required becomes 5×10^{5} ℓ/s, which is marginally an engineering possibility. The pumped limiter experiment by Overskei [4] suggests that a mechanical divertor approach might work, but no experiment has fully demonstrated this capability for a helium ash exhaust.

Helium enrichment is also important from the viewpoint of tritium inventory. If the ratio of the helium density to the fuel density at the pump duct is low compared to that in the hot plasma core, much fuel must be pumped out in order to pump a definite amount of helium. This situation is undesirable since the cryopumps most be regenerated frequently, which limits the duty cycle of the fusion reactor. The tritium inventory on the cryopanels is limited by: 1) heat load on the cryopanels due to tritium decay, 2) safety requirements, and 3) cost [5].

5.2 Helium Exhaust Experiment

We wanted to test by experiments the feasibility of using a divertor to concentrate neutral helium in divertor plasmas in Doublet III. Figure 5.1 shows the experimental setup. The diverted plasma is formed in the upper half of the Doublet III vacuum vessel. This simplified divertor has the divertor coils outside the vacuum vessel and there is no special divertor chamber or divertor throat. Helium gas is injected into the vacuum vessel from the upper port in a pulse of 5 msec duration at the time of ~ 600 msec in the hydrogen discharge. The discharge lasts for 900 msec. The amount of helium gas corresponds to a helium particle density of 1.1×10^{13} cm^{-3} if it were distributed uniformly in the plasma.

A quadrupole mass analyzer installed at the lower chamber port is used to monitor neutral helium pressure during and after the discharge. Ionization gauges are used to detect the total pressure (hydrogen molecule pressure) near the main plasma and in the lower chamber. The vacuum time constants of this mass analyzer and ionization gauges are ~ 100 msec. The density of helium ions in the main plasma is obtained from the difference in electron density Δn_e of the two otherwise similar discharges; one with helium injection, the other without helium. To simulate an alpha-heated tokamak, the measurements are made after the helium pressure reaches equilibrium levels ($\gtrsim$ 200 ms after the helium gas puff). Figure 5.2 shows the hydrogen and helium partial pressure as a function of density with and without divertor. For diverted discharges, both the hydrogen and helium pressure at the lower chamber are strongly increasing functions of density and reach values up to 4.1×10^{-3} and 9.6×10^{-5} Torr. Figure 5.2 also shows that the ratio of hydrogen pressure at

the lower chamber to the pressure near the main plasma increases with the increase of density and this ratio attains values up to ~ 300 at high density. On the other hand, the pressure of helium without a divertor is lower by one order of magnitude than that with a divertor. Hydrogen pressure at the lower chamber is observed to be about the same as that near the main plasma in the non-diverted discharges.

Figure 5.3 compares the increment in $\bar{n}_e$ with helium injection for discharges with and without divertor. From this measurement, the concentration of helium ions in the main plasma (deduced as $\Delta\bar{n}_e/2$) for diverted discharges is lower than that for non-diverted discharges. For the highest density diverted discharge, the concentration of helium ions in the main plasma is ~ 1.6% of $\bar{n}_e$. This result shows that helium pressure of 9.6×10^{-5} Torr is attained in the lower chamber with a helium concentration of 8.2×10^{11} cm^{-3} in the main plasma.

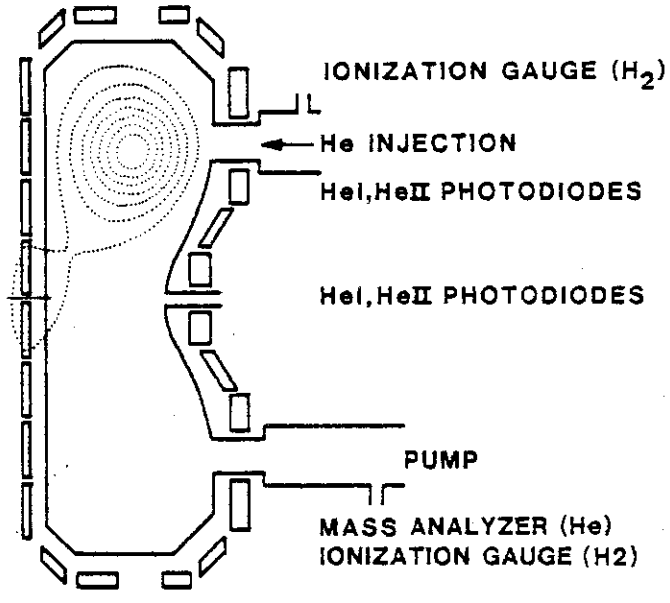

FIG. 5.1 Diagnostics and impurity injection system are shown with a divertor configuration with open geometry (no divertor throat, no divertor chamber, divertor coils outside the vacuum vessel).

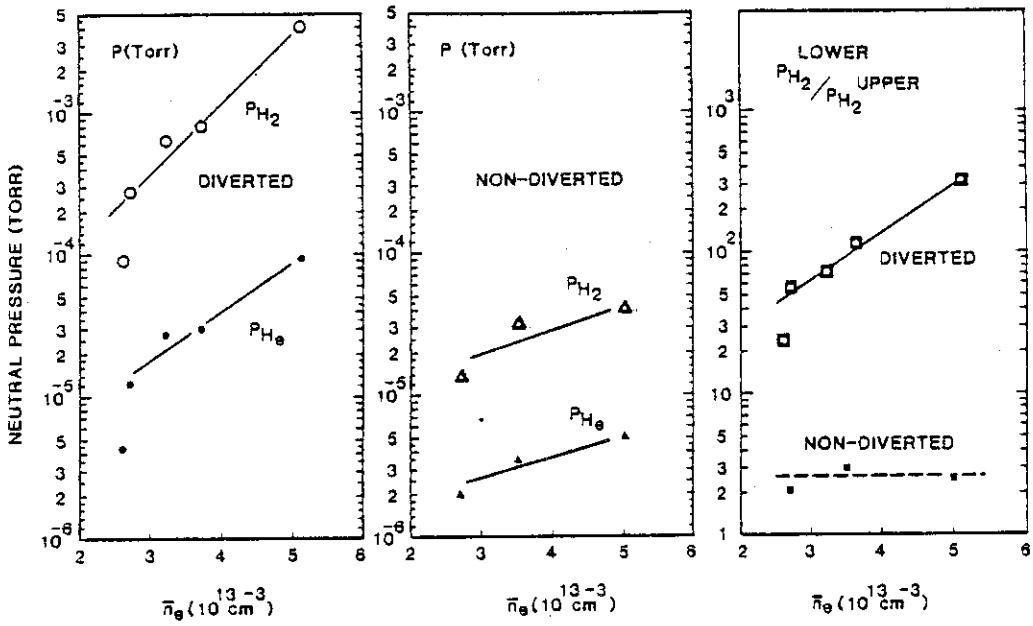

FIG. 5.2 Pressure of molecule hydrogen and helium measured at the lower chamber ports vs. electron density with and without divertor (measured just before the helium gas puff). The ratio of P_{H_2} measured at the lower chamber port to P_{H_2} near the main plasma is also shown. In a high density divertor discharge, P_{He} reaches ~ 1 x 10^{-4} Torr with a helium concentration of 1.6% in the main plasma. This result demonstrates the effective ash exhaust function of a divertor.

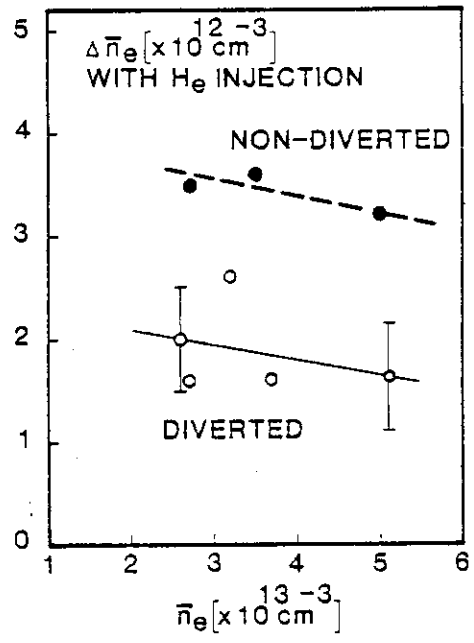

FIG. 5.3 The increment of electron density after helium injection vs. $\bar{n}_e$ (measured just before the helium gas-puff).

5.3 Discussions and Application to INTOR-grade Large-scale Devices

There was some concern that most of the injected helium particles are directly swept out to the divertor region so that this experiment does not simulate an alpha-particle-heated tokamak in which helium is generated in the hot core. In order to clarify this problem, helium gas is injected before the divertor is turned on. However, the helium density in the lower chamber has shown no difference from the case in which helium atoms are injected after the divertor is turned on. Therefore, the experiments presented in this dissertation may be recognized as those simulating an alpha-particle-heated plasma.

The helium enrichment is another key factor of ash exhaust from the viewpoint of tritium inventory. The helium enrichment factor is defined by:

$$\eta = (P_{H_e}/2P_{H_2})_{\text{lower chamber}} \Big/ (\overline{n}_{H_e}/\overline{n}_e)_{\text{main plasma}}$$

As is discussed in §5.1, a high value of $(P_{H_e}/2P_{H_2})$ at the pump duct with a low value of (n_{H_e}/n_e) is favorable from the viewpoint of exhaust efficiency and reactor performance. Therefore, the higher the η is, the easier helium exhaust becomes. η is presented in Fig. 5.4 as a function of the average electron density in the main plasma volume, $\overline{n}_e$. The helium enrichment factor is found to be an almost constant for variation in $\overline{n}_e$, with a range of values $0.5 < \eta < 1.0$. This result shows that compression of hydrogen and helium neutrals in the lower chamber are similar. That is, neither strong helium enrichment [1, 2, 3] nor de-enrichment [6] is found. η in non-diverted discharges is found in is found in the range $1.0 < \eta < 2.0$ showing a slight

enrichment. However, it is difficult to assess the feasibility of a mechanical divertor from this result, since the pressure is measured far from the limiter in this particular experiment.

The helium compression realized in the present experiment is large enough to be applied to reacting-plasma-grade devices like INTOR, where the helium allowance of 5% of $\bar{n}_e$ ($\bar{n}_e = 1.2 \times 10^{14}$ cm^{-3}) is assumed. If we simply scale the prsent experimental results, a helium pressure of 7.1×10^{-4} Torr will be obtained in INTOR. The required pumping speed becomes 7.0×10^3 ℓ/s. This value relxes the presently proposed pumping speed design for INTOR by a factor of 70.

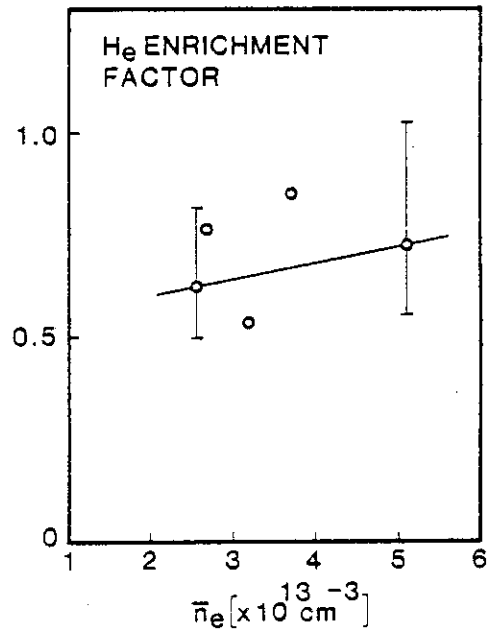

FIG. 5.4 Helium enrichment factor η defined by:

$$\eta = (P_{He}/2P_{H2})_{\text{lower chamber}} \; / \; (\bar{n}_{He}/\bar{n}_e)_{\text{main plasma}}$$

is $0.5 < \eta < 1.0$ with divertor. ($\bar{n}_{He}$ derived by $\Delta\bar{n}_e/2$).

5.4 Summary of Chapter 5

The conclusions are summarized as follows:

1. Without any divertor chamber or divertor throat, neutral helium is concentrated at the divertor region with pressure up to 1.0×10^{-4} Torr with a helium concentration of 1.6% of elecron density in the main plasma. No strong enrichment or de-enrichment of helium is found in the divertor region.
2. Helium pressure in the lower chamber without divertor is lower than that with divertor by one order of magnitude.
3. Helium ash exhaust is realistic in an alpha-particle-heated diverted tokamak.

REFERENCES (Chapter 5)

[1] SHIMOMURA, Y. SAKO, K., SHINYA, K., "Some Consideration of Ash Enrichment and Ash Exhaust by a Simple Divertor", Japan Atomic Energy Research Institute Report No. JAERI-M8294 (1979).

[2] TAKIZUKA, T., AZUMI, M., SEKI, Y., SENGOKU, S., MAKI, K., et al., in Plasma Physics and Controlled Nuclear Fusion Research (Proc. 8th Int. Conf. Brussels, 1980) Vol. 2, IAEA, Vienna (1981) 679.

[3] SEKI, Y., SHIMOMURA, Y., MAKI, K., AZUMI, M., TAKIZUKA, T., Nucl. Fusion 20, 1213 (1980).

[4] OVERSKEI, D., Phys. Rev. Lett. 46, 177 (1981).

[5] FUSION RESEARCH AND DEVELOPMENT CENTER, "INTOR WORKSHOP REPORT, Group 14 -- Vacuum --", Japan Atomic Energy Research Institute Report No. JAERI-M8513 (1979).

[6] CALLEN, J. D., EMMERT, G. A., BAILEY, A. M., BENCHIKH-LEHOCINE, M. E., DAVIDSON, J. N., et al., in Plasma Physics and Controlled Nuclear Fusion Research (Proc. 8th Int. Conf. Brussels, 1980) Vol. 2, IAEA, Vienna (1981) 775.

6. Remote Radiative Cooling by Divertor

6.1 Erosion and Heat Load Problems in INTOR Reactor Design [1]

In a high temperature reacting-plasma-grade, large-scale machine like INTOR, a heat flux of as much as 80 MW and a particle flux of as much as 2 x 10^{21}/sec are transported onto the divertor plates in diverted mode, and onto the limiter and first wall in non-diverted mode. Handling of this heat and particle flux is a major concern in the reactor design. The design of the divertor plates is one of the cruxes of INTOR design study. The divertor plates are exposed to heat flux density of 200 W/cm^2, and particle flux density of 1.5 x 10^{16}/cm^2/sec with particle energy of 100 -400 eV. Initial design study showed that the stainless-steel divertor plates' erosion rate is 25 cm/yr. Recent design study employs tungsten which is costly and hard to fabricate and becomes brittle after recrystallization. In order to effectively remove high heat flux, the structure becomes complicated. The time and effort required for fabrication of the divertor plates and their replacement every 2 years are cumbersome. The same difficulty is true for the limiter design.

If the heat flux can be reduced to 50 W/cm^2, and the electron temperature can be cooled down to ~ 10 eV, the technical difficulties in the divertor plates are much eased. Moreover, if the erosion and heat load problems of the divertor plates are solved in a diverted tokamak, the divertor provides a solution of the erosion and heat load problems of the first wall and the limiter.

6.2 Remote Radiative Cooling

Figure 6.1 shows the vertical distribution of radiation (combination of line radiation and charge-exchange neutral power) measured with a 21-channel bolometer-array which views the entire main plasma and divertor region. The viewing cone of each channel of the bolometer array is also shown in the figure. With the increase of density, radiation from the divertor region increases while the radiation from the main plasma is relatively constant. Assuming vertical symmetry in the radiation power of the main plasma, we can subtract the contribution of the main plasma from the power flux to the bolometer looking at the divertor. The radiation power density in the divertor region reaches levels up to ~ 0.3 W/cm^3 (with the horizontal width of the radiating layer assumed to be ~ 20 cm). This experimental result demonstrates remote radiative cooling such as heat transported along the scrape-off field lines to the divertor is radiated before reaching the divertor plate.

We shall discuss the source of this radiation power in the divertor. The impurities present in Doublet III are metallic impurities (Ni, Ti, Cr) and light impurities (O, and C). We can eliminate the possibility of metallic impurities and carbon as follows:

The abundance of nickel ions in the main plasma is spectroscopically deduced to be $\sim 10^{-6}$ of electron density. For the condition in the divertor ($n_e \simeq 5 \times 10^{13}$ cm^{-3}, $T_e < 20$ eV, particle recycling time ~ 1 msec) the radiation power from nickel is calculated (in a similar fashion to the oxygen radiative power calculation described in the Appendix 1) to be $\sim 10^{-4}$ W/cm^3,

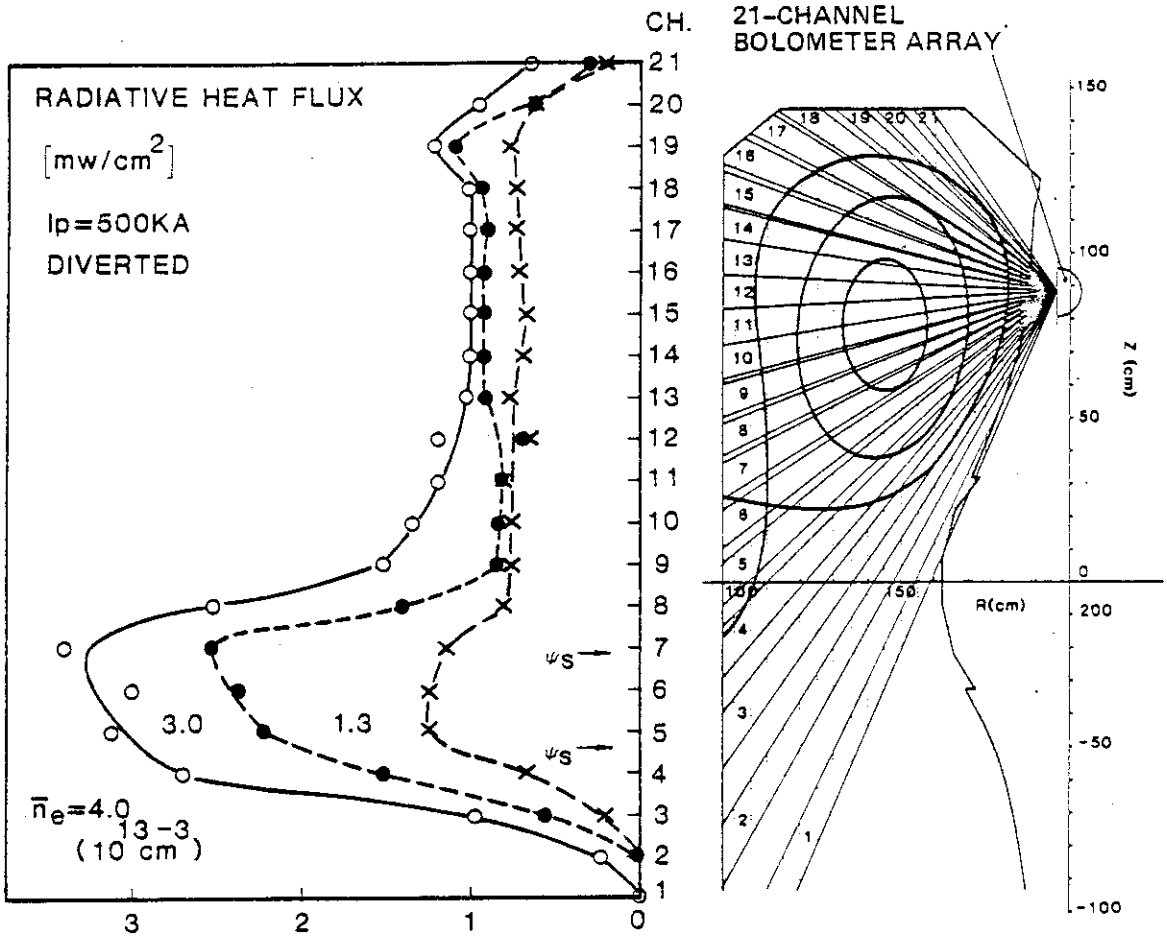

FIG. 6.1 Line-integrated radiation power profile for three different $\bar{n}_e$. The location of the 21-channel bolometer array, and the viewing-cone of each collimated detector are indicated in the figure. With the increase of $\bar{n}_e$, the radiation from the divertor region increases while the radiation from the main plasma is kept almost constant.

if a nickel concentration of 10^{-6} is assumed in the divertor. Other metallic impurities can be similarly eliminated from the candidates.

From the measured line intensity of C IV, the radiation power from this lithium-like ion is ~ 3 kW in non-diverted discharges. Carbon is not likely to radiate much power in the divertor, because carbon is a minor impurity even without the divertor.

Figure 6.2 shows H_α, O I, P_{rr} as a function of $\bar{n}_e$ where O I corresponds to the O I 7773Å intensity and H_α corresponds to H_α line intensity with both measured at the radial chord intersecting the divertor region. The data was taken when the vacuum vessel is well conditioned (clean) and relatively dirty for the sake of comparison. The H_α line intensity is proportional within a factor of two to the Lyman series radiative power for the parameter range investigated here. It is difficult to deduce the radiative power of oxygen from the line intensity of O I 7773Å. We simply assumed here that the line intensity of O I 7773Å is roughly proportional to the oxygen line radiation. This graph suggests that neutral hydrogen contributes most to the remote cooling power in the clean condition, and oxygen emits most of the radiation power in the dirty condition. This situation is clearly seen in Fig. 6.3, where OI/P_{rr} is shown as a function of H_α/P_{rr}. The data suggest that $P_{rr} \propto OI + H_\alpha$, i.e., the source of the remote radiative cooling is hydrogen and oxygen line radiation.

From the measured intensity of $H_\alpha \sim 9 \times 10^{15}$ photon/cm^3/sec at the pure hydrogen radiation case in the figure, the line radiation of the Lyman series

is estimated [2] to be ~ 0.3 W/cm^3, which is in reasonable agreement with the bolometer measurement of ~ 0.3W/cm^3 in the divertor region (Fig. 6.1). It is more difficult to deduce the oxygen concentration in the divertor plasma from the O I 7773Å line intensity. However, on the basis of the simple non-coronal model (see Appendix 1) the measured radiation power density of 0.3 W/cm^3, is consistent with that of ~ 1% oxygen concentration in a plasma of n_e = 5 x 10^{13} cm^{-3} and T_e = 5 eV. Since the Z_{eff} of the main plasma is ~ 1.1 -1.5, an oxygen concentration of ~ 1% in the divertor region appears to be reasonable.

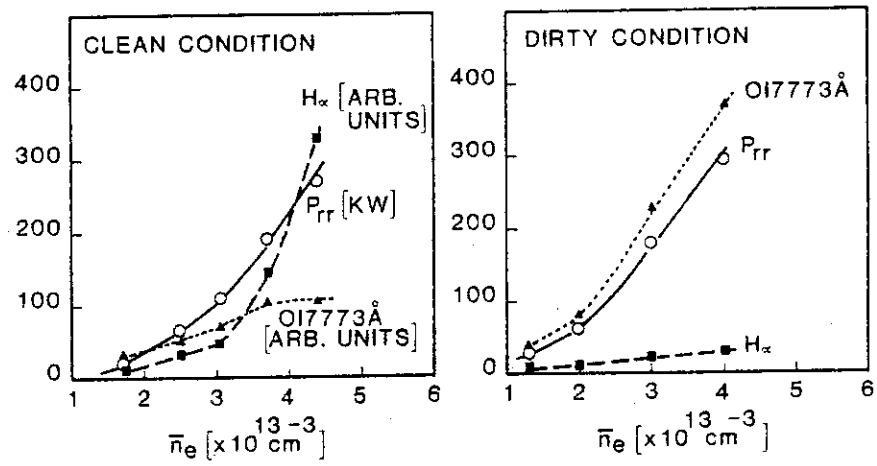

FIG. 6.2 Line intensities of H_α and O I 7773Å in the divertor, and remote radiative cooling power P_{rr} as a function of $\bar{n}_e$.

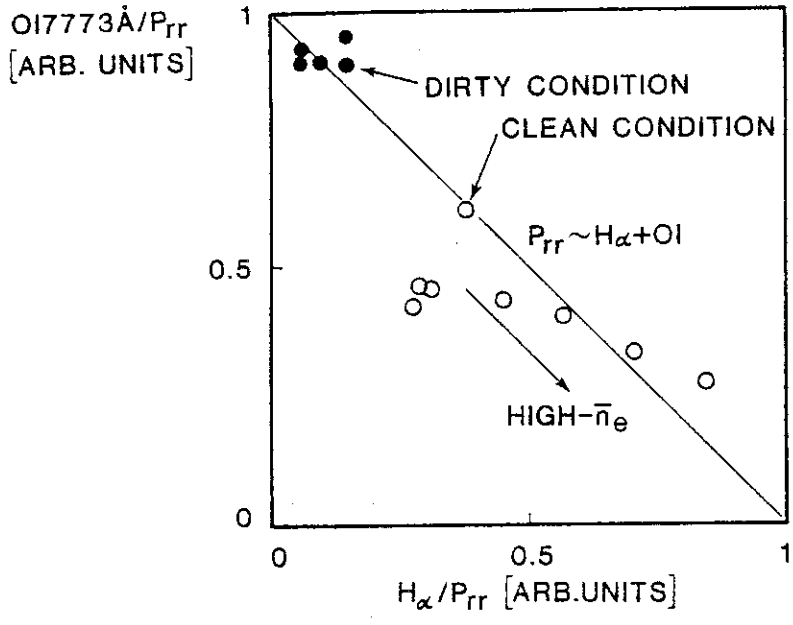

FIG. 6.3 OI/P_{rr} (the line intensity of O I 7773Å divided by remote radiative cooling power P_{rr}) as a function of H_α/P_{rr} (H_α line intensity divided by P_{rr}). The origin of remote radiation is mainly the line radiation of oxygen and hydrogen.

6.3 Formation of Dense and Cold Divertor Plasma by Remote Radiative Cooling

The cooling of the divertor plasma by radiation is shown in Fig. 6.4 which shows the spatial distribution of O I 7773Å, O II 4416Å and C III 4649Å line emissions from a filtered TV which looks tangentially at the divertor region. For low-density discharges, the origin of emissions is located around the separatrix field line near the inside wall. For high density discharges, however, the origin of O II and C III emissions moves from the inside wall region to the main plasma region, while O I emission remains localized to the separatrix surface near the wall.

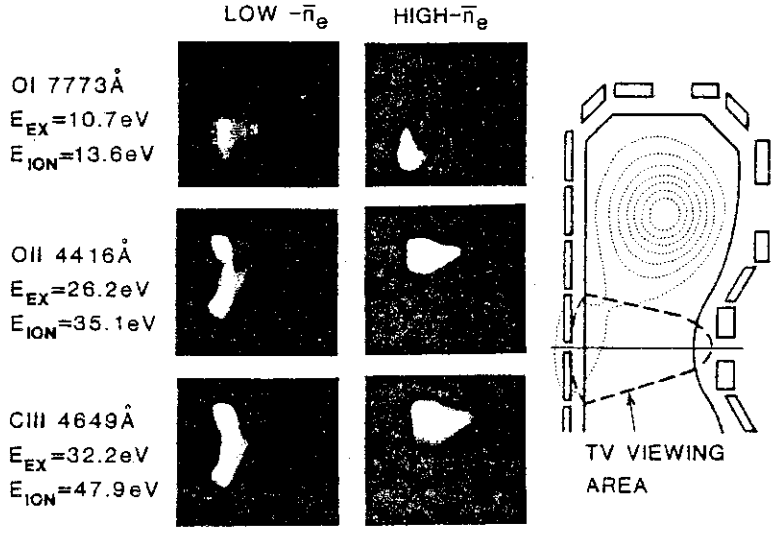

FIG. 6.4 Two-dimensional maps of O I, O II, C III visible line emission in the divertor for the low $\bar{n}_e$ case and high $\bar{n}_e$ case. Change of the location of O II and C III line emission in low-$\bar{n}_e$ to high-$\bar{n}_e$ suggests that the divertor plasma is cooled down to less than 10 eV.

Taking into account the ionization energy (O I 13.6 eV, O II 35 eV, C III 48 eV) as well as excitation energy (O I 10.7 eV, O II 26 eV, C III 32 eV), this observation indicates that the electron temperature near the wall is high enough to have multiple ionization for low density discharges, and is too low to ionize O I or to excite the O II line for high density discharges. We may infer that the location of the line emission is determined by the balance of the particle confinement time (~ 1 msec) and the ionization time.* note) The ionization time τ_{ion} of O II changes greatly with T_e between 5 - 10 eV; τ_{ion} = 0.05 ms at T_e = 10 eV and τ_{ion} = 20 msec at T_e = 5 eV with $n_{e_{DIV}} = 5 \times 10^{13}$ cm^{-3}. τ_{ion} = 1 msec corresponds to T_e = 7 eV. Therefore, because the burn-out of OII**note) occurs near the main plasma for high density discharges, the T_e at the center of the divertor region (center of the TV view) should be less than 10 eV and probably be ~ 7 eV.

The neutral temperature in the divertor region is measured through the doppler-broadening of the H_α-line and is found to be 1 -2 eV in the high density discharges . A clear Zeeman-splitting of the H_α line is also observed. This is utilized to determine that the H_α radiation is peaked at ~ 13 cm from the inside wall, which corresponds to the location of the separatrix field line. Since the charge-exchange process is more frequent than the wall recombination when $n_e > 5 \times 10^{13}$ cm^{-3} (where the mean-free-path of neutral particles for the charge-exchange is less than 3 cm), the neutral particles should be equilibriated with protons near the separatrix surface. Thus, it appears that the remote radiation effect cools the diverted plasma to the level of 1 -7 eV.

---

*note : mean-free-time of electron-impact ionization

**note : ionization to higher ionization states

6.4 Reduction of Heat Load to Divertor Plate by Remote Radiative Cooling

Figure 6.5 shows the power balance for a diverted discharge of I_p = 500kA. For increasing plasma density, the radiative loss in the main plasma, P_r, exhibits no drastic change (around $P_r/P_{OH} \sim 20$ -30%), while the remote radiation P_{rr} in the divertor region increases up to $P_{rr}/P_{OH} \sim 50\%$. At the same time, the heat flux to the divertor plates, as measured with thermocouples and an infrared (IR) camera, decreases. The peak heat-load of the divertor plate (ϕ_{div}) is observed to decrease as the remote radiative cooling power (P_{rr}) increases (Fig. 6.6). The total vertical extent of the heat flow to the divertor plate in high density discharges is ~ 40 cm around the intersection of the upper and lower separatrix field line with the wall.

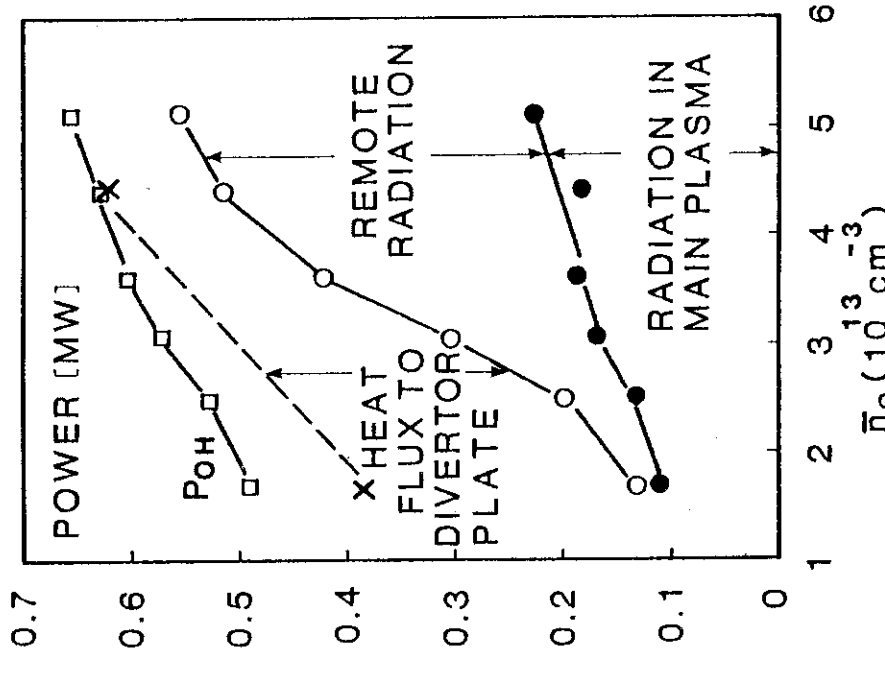

FIG. 6.5 Power balance of diverted discharges of I_p = 500 kA. Ohmic input power P_{OH}, radiation power in the main plasma P_r, remote radiative cooling power P_{rr} as a function of $\bar{n}_e$. The power to the divertor plates measured by thermocouples are also shown in the figure. The remote radiation reaches ~ 50% of ohmic input at high $\bar{n}_e$.

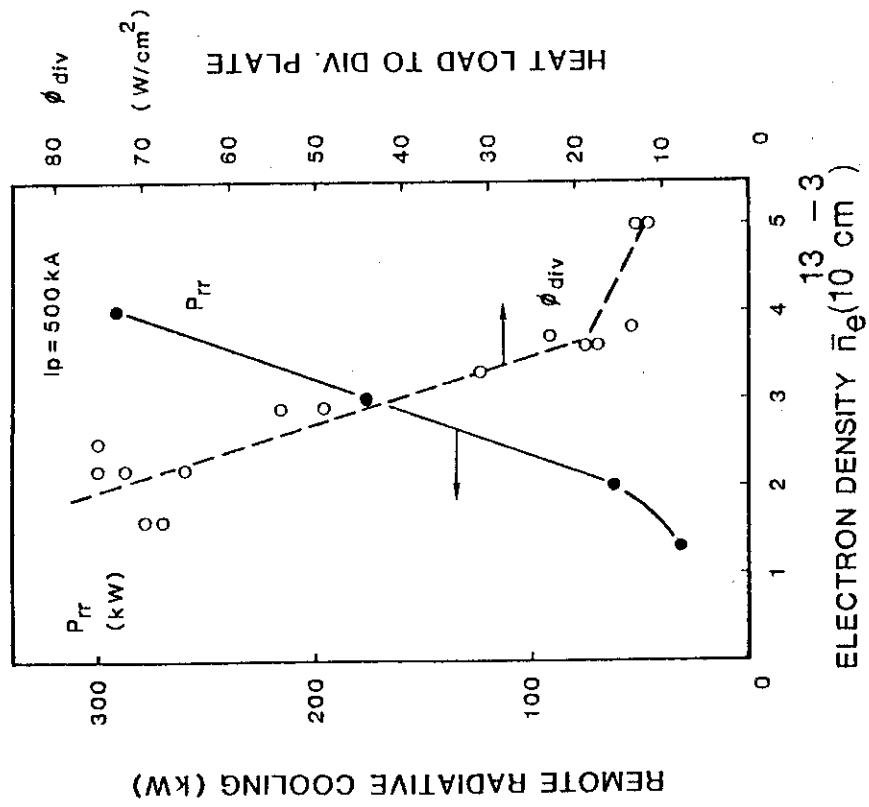

FIG. 6.6 The peak heat load of the divertor plate ϕ_{DIV} and remote radiative cooling power P_{rr} as a function of $\bar{n}_e$. The peak heat load of the divertor plate ϕ_{DIV} is significantly reduced by the increase of remote radiative cooling power P_{rr}.

6.5 One-dimensional Heat Conduction Calculation of Radiative Divertor Plasma

A one-dimensional heat flow equation along the scrape-off field line with radiative cooling by oxygen was solved and the result shows a sufficient cooling of the divertor plasma. The equations are [3]

$$\nabla_{\parallel} (K_{\parallel} \nabla_{\parallel} T_e) = P_{r_{DIV}}, \qquad \text{(Power balance)}$$

$$\nabla_{\parallel}(n_e T_e) = 0. \qquad \text{(Constant pressure)}$$

Here, the heat flow is assumed to be dominated by heat conduction, and the electron pressure is assumed to be constant along the field line. There is a possibility that these approximations are inadequate near the divertor plate, where particle-recycling intervenes, and the resultant convective loss, momentum-transfer between protons and neutrals and the effect of electric field may become important. Moreover, the ionization, charge-exchange and radiation loss of hydrogen neutrals are not taken into account. Full inclusion of these effects is the subject of future study.

The boundary conditions for heat flow are:

1) $-Bp/B_T \bullet S K_{\parallel} \nabla_{\parallel} T_e = P_{OH} - P_r$ (power balance at the main plasma edge),

2) and $-K_{\parallel} \nabla_{\parallel} T_e = \gamma \Gamma T_e$ (power balance at the divertor plate),

where B_p/B_T is the pitch of the field line, $K_{\parallel}$ the parallel electron heat conduction coefficient [4], S the cross-sectional area of the divertor scrape-off, γ the particle heat transmission coefficient (= 7.8) and the particle flux $\Gamma = 0.3\ Cs\ n_e$ [5].

Figure 6.7 is a typical computational result showing the T_e, n_e, $P_{r_{DIV}}$ profiles along the field line for the 1% oxygen level and $P_{OH} - P_r$ = 300 kW. For an electron density at the edge of the main plasma of n_{e_b} = 1.2 x 10^{13} cm^{-3} ($\bar{n}_e \sim 5 \times 10^{13}$ cm^{-3}), the average $P_{r_{DIV}}$ attains ~ 0.3 W/cm^3. The divertor plasma is cooled from 27 eV near the main plasma down to 1 eV at the divertor plate. The electron density near the divertor plate exceeds 5 x 10^{13} cm^{-3}. The total remote radiation power is as much as 80 % of $P_{OH} - P_r$. In a lower plasma density case with n_{e_b} = 0.4 x 10^{13} cm^{-3} ($\bar{n}_e \sim 2 \times 10^{13}$ cm^{-3}), n_e and T_e are approximately constant along the field line. This simple calculation clearly shows the effectiveness of radiative cooling in the formation of a dense and cool divertor plasma.

If this remote radiative cooling scheme can be applied to a tokamak reactor like INTOR, the problems of high heat load, and high erosion rate of the divertor plate will be significantly reduced. Moreover, an attractive feature of this edge cooling scheme is clearly seen in Fig. 6.7. While the electron temperature near the divertor plate is cooled from ~ 50 eV in the low density case to ~ 1 eV in high density case, the electron temperature of the main plasma edge changes little (from slightly less than 50 eV to 27 eV). Therefore, the divertor plasma is cooled without cooling the main plasma edge. This feature is attractive from the viewpoint of plasma stability. The feasibility of remote radiative cooling in INTOR is discussed in the next section.

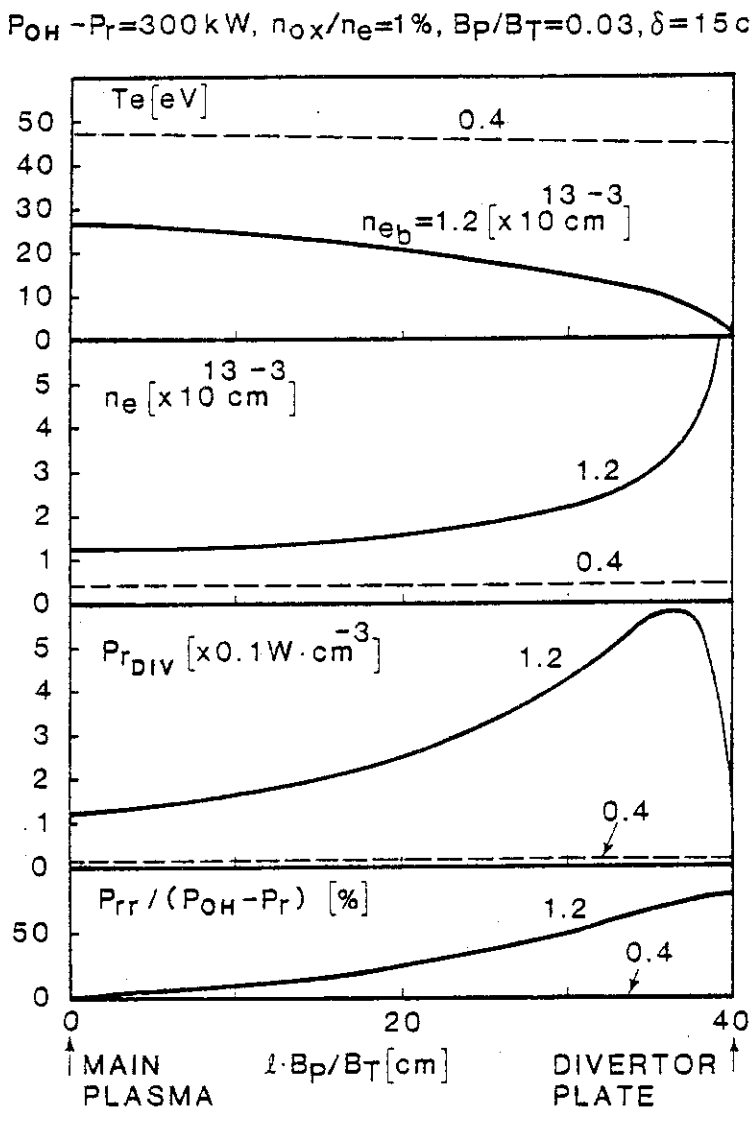

FIG. 6.7 T_e, n_e, $P_{r_{DIV}}$ (radiation power density) profiles along the field line in the divertor.

6.6 Possibility of Remote Radiative Cooling in INTOR

A method of integrating the radiation power along the field line is presented in this chapter, and is utilized to estimate the impurity concentration in the divertor necessary to dissipate the power which flows from the main plasma into the divertor for typical INTOR parameters.
The heat conduction equation along the field line is

$$Q = -K_{\parallel} \frac{dT}{dx} \tag{1}$$

$$\frac{dQ}{dx} = -P_{r_{DIV}} \tag{2}$$

where Q is the heat flux density,

T is the electron temperature,

x is the coordinate along the field line.

The product of eqs. (1) and (2) yields

$$\frac{Q_b^2}{2} - \frac{Q_d^2}{2} = \int_{T_d}^{T_b} K_{\parallel} P_{r_{DIV}} \, dT \tag{3}$$

where the subscripts b and d represent the main plasma edge, and the divertor plate, respectively.

Here, the quantities $K_{\parallel}$ and P_{rDIV} may be written as

$$\left.\begin{aligned} K_{\parallel} &= K_o\, T^{\frac{5}{2}} \qquad (K_o = 12.5\ \mathrm{W/cm/(eV)^{7/2}}\ [4]) \\ &\text{and} \\ P_{r_{DIV}} &= n\, n_z\, L(T) \\ &= n^2 f L(T) \\ &= p^2\, f\, \frac{L(T)}{T^2} \end{aligned}\right\} \quad (4)$$

where n : electron density,

n_z : impurity atom density,

$L(T)$: radiative cooling rate,

and f denotes the ratio n_z/n, and

p the electron gas pressure.

Only the line radiation by impurity is included in L(T). The line radiation, charge-exchange and ionization power of the fuel particles are not taken into account.

we make the following two assumptions:

1) p is constant along the field line, and

2) f is constant along the field line.

then eq. (3) and expressions (4) lead to

$$Q_b^2 - Q_d^2 = p^2 f \left[g(T_b) - g(T_d) \right] \tag{5}$$

where

$$g(T) = 2K_o \int_o^T L(T) \sqrt{T} \, dT \tag{6}$$

The radiative cooling rate L(T) may be calculated once $n\tau$ (τ is the recycling time) is specified (see Appendix1).

Figures 6.8 and 6.9 show the values of g(T) for oxygen and argon. From these figures it is seen that g(T) is a strong function of electron temperature. For example, for $T_b > 40$ eV, and $T_d < 10$ eV, the relation $g(T_b) \gg g(T_d)$ holds. Therefore, if $T_b > 40$ eV (which appears to be a typical electron temperature condition of the tokamak-reactor edge) $Q_b \gg Q_d$, and $Q_b^2 \sim p^2 f\, g(T_b)$, then T_d becomes low ($\lesssim$ 10 eV) and n_d becomes high.

Now, let us define f_o as

$$f_o = \frac{Q_b^2}{p^2 \, g(T_b)} \tag{7}$$

which stands for a measure of the impurity concentration.

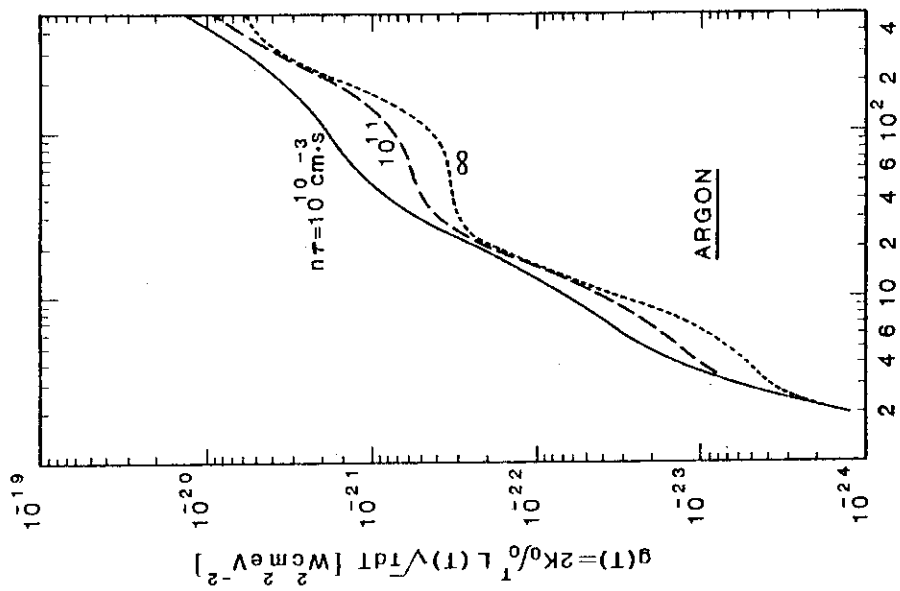

FIG. 6.9 g(T) vs. T_e for argon. $n\tau$ is the electron density multiplied by the recycling time of the impurity particles.

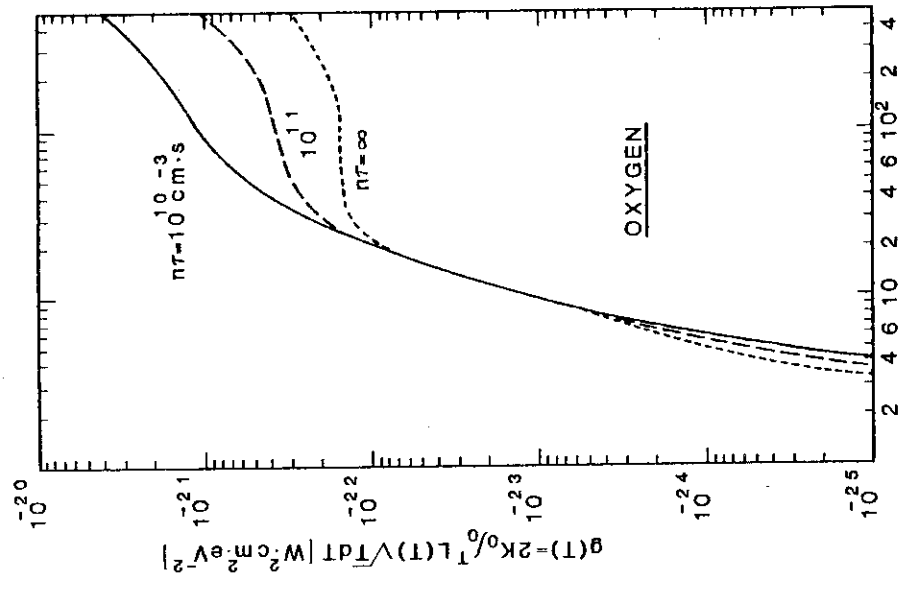

FIG. 6.8 g(T) vs. T_e for oxygen, $n\tau$ is the electron density multiplied by the recycling time of the impurity particles.

From eq. (7), we can calculate the impurity concentration f_o which is required to radiate ~ 100% of the power (Q_a) from the main plasma and in turn, to make a dense and cold divertor plasma.

The standard parameters of the INTOR divertor are [1]:

R = 500 cm (major radius)

P = $P_\alpha - P_r$ = 80 MW (power from the hot core)

d = 100 cm (length of the divertor)

δ = 15 cm (thickness of the scrape-off layer)

Θ = B_p/B_T = 0.05 (pitch of the field line)

n_b = 5×10^{13} cm^{-3} (electron density at the divertor entrance)

$$Q_b = \frac{P}{4\pi R\delta\Theta} = 1.7 \times 10^4 \text{ W/cm}^2$$

$$\ell = \frac{d}{\Theta} = 2 \times 10^3 \text{ cm}$$

ℓ is the distance from the main plasma edge to the divertor plate along the field line.

T_b is approximately given by Ref. [6] to be

$$T_b \simeq \left(\frac{7}{2}\,\frac{Q_b}{K_o}\,\ell\right)^{\frac{2}{7}} \simeq 100 \text{ eV}, \quad \text{and}$$

$$p = n_b T_b = 5 \times 10^{15} \text{ cm}^{-3} \text{ eV}.$$

If we choose $n\tau$ to be 10^{11} $cm^{-3} \cdot s$,

$$f_o = \frac{Q^2_b}{p^2\, g(T_b)} = 3.3\% \text{ for oxygen and } 1.6\% \text{ for argon.}$$

Next, the parameter dependence of f_o on n_b, $n\tau$, and δ are studied, because these quantities are difficult to predict with good accuracy.

Figures 6.10 and 6.11 show the dependence of f_o on n_b and $n\tau$. The dependence on n_b is

$$f_o \propto \frac{1}{n_b{}^2}$$

The recycling-time τ is short for the intensive recycling condition. For a smaller $n\tau$, the ionization stage is lower, which enhances L(T). The dependence of f_o on $n\tau$ is approximately $\propto (n\tau)^{0.3}$.

The f_o-values scale like $\propto \delta^{-1.4}$ as shown in Fig. 6.12 (oxygen) and Fig. 6.13 (argon). The scaling is expressed as follows:

$$T_b \propto \delta^{-2/7} \text{ since } Q_b \propto \delta^{-1} \text{ and } T_b \propto Q_b^{2/7}, \text{ and}$$

$$f \propto \frac{Q_b{}^2}{T_b{}^2}\, g(T_b)^{-1}$$

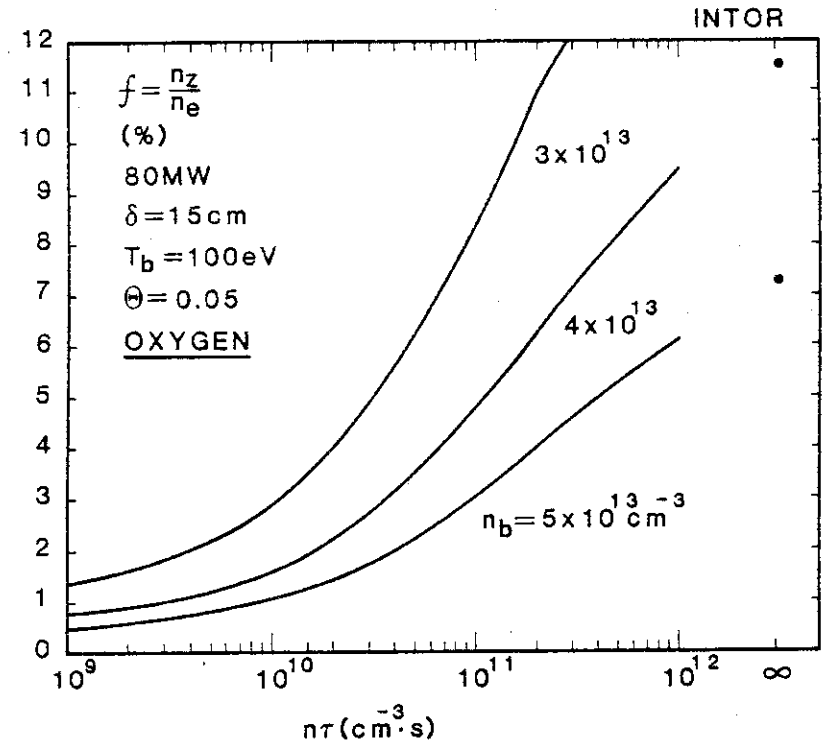

FIG. 6.10 f vs. nτ (oxygen). f is the impurity concentration (= n_z/n_e) necessary to radiate ~ 100% of the heat flux from the main plasma. n_b is the electron density at the divertor entrance.

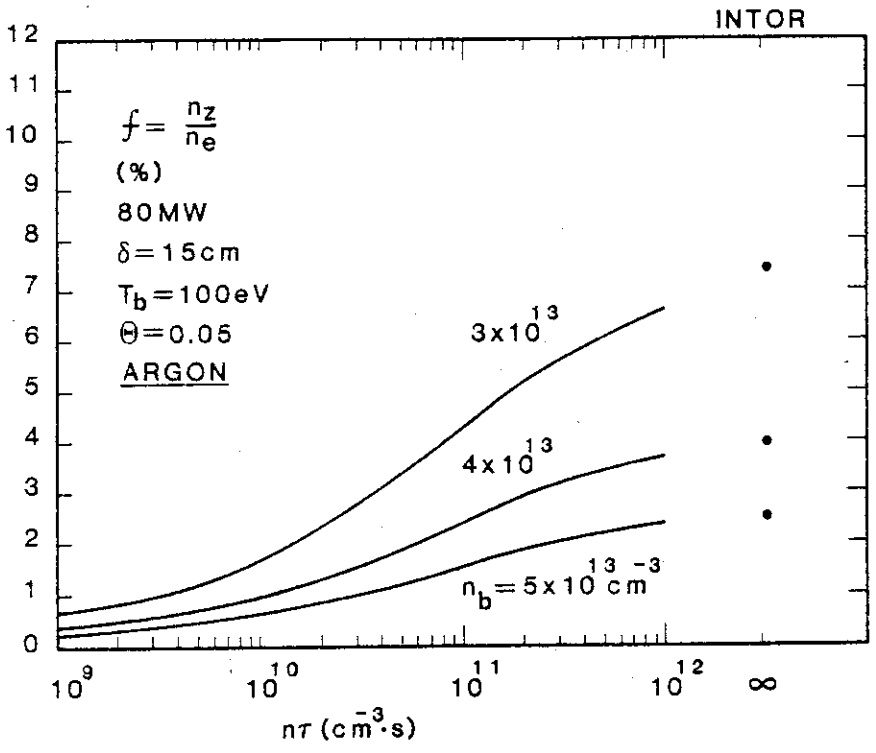

FIG. 6.11 f vs. nτ (argon). f is the impurity concentration (= n_z/n_e) necessary to radiate ~ 100% of the heat flux from the main plasma. n_b is the electron density at the divertor entrance.

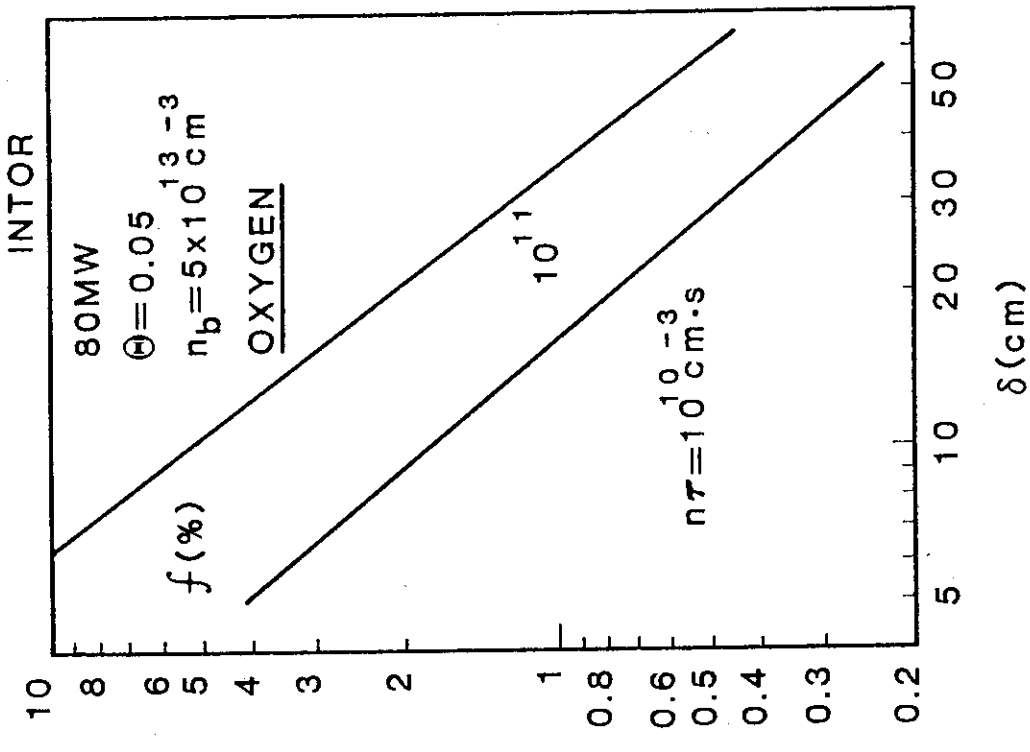

FIG. 6.12 f vs. δ (oxygen). δ is the width of the scrape-off layer in the divertor.

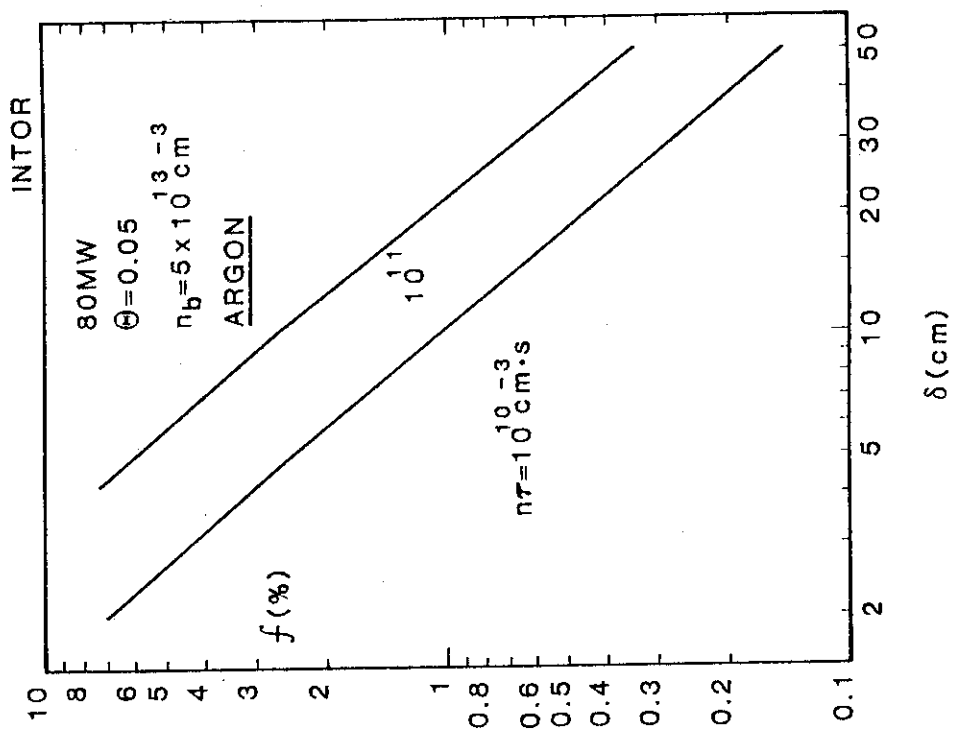

FIG. 6.13 f vs. δ (argon). δ is the width of the scrape-off layer in the divertor.

Accordingly,

$$f \propto \delta^{-2} \cdot \delta^{4/7} \simeq \delta^{-1.4}$$

as g(T) is almost constant for $40 < T_b < 100$ eV.

The calculated results on INTOR are summarized as follows:
If we allow 3% oxygen into the divertor, it is possible to radiate ~ 100% of the power flow into the divertor by oxygen line radiation under a condition of $n\tau \lesssim 10^{11}$ cm^{-3} · s , $n_b \gtrsim 4 \times 10^{13}$ cm^{-3}, $\delta \gtrsim 15$ cm.
If we allow the argon impurity concentration to be ~ 3% in the divertor, argon will radiate ~ 100% of the power flow into the divertor under a condition of $n\tau < 10^{12}$ cm^{-3} · s, $n_b \gtrsim 4 \times 10^{13}$ cm^{-3}, $\delta \gtrsim 5$ cm.

It is necessary to note that our model is preliminary in the sense that we do not include hydrogen neutral recycling and radiation. As has already been discussed in §6.2, the Lyman-series line-radiation estimated from the measured H_α-line intensity is strong enough to explain the radiative power in the divertor in Doublet-III. The inclusion of this effect will reduce the f_o-values obtained here. Moreover, even if we allow 3 % of impurities in the divertor, the impurity concentration in the main plasma can be maintained at a much lower level. In the DIVA case, only 0.3 % of the metallic impurity influx into the divertor was observed to penetrate into the main plasma [7]. A high efficiency argon exhaust by a divertor is observed by General Atomic Expanded Boundary Group [8].

6.7 Summary of Chapter 6

1) High-density diverted discharges provide strong accumulation of particles and enhanced recycling in the divertor region. This results in a strong radiative cooling of the diverted plasma. The radiated power in the divertor accounts for as much as 50% of the ohmic input power, thus effectively cooling the plasma in front of the divertor plate down to several eV. This remote radiative cooling greatly reduces the heat load on the divertor plate without cooling the main plasma. This operating scheme could well reduce the sputtering, erosion and heat removal problems of divertor plates in future reactors.

2) A one-dimensional numerical simulation of the radiative divertor elucidates the effect of remote radiative cooling process on the formation of the dense and cold divertor plasma.

3) A simple calculation for the INTOR divertor predicts that effective remote radiative cooling appears to be possible with an intentional minor injection of oxygen and argon gases into the divertor region.

REFERENCES (Chapter 6)

[1] INTOR group, "International Tokamak Reactor - Phase One" IAEA, Vienna (1981) to be published.

[2] JOHNSON, L. C., Astrophys. J. 174 (1972) 227.

[3] TENNEY, F. H., LEWIN, G., in "A Fusion Power Plant", Chap. 6 (ed. by Mills, R. G.,) MATT-1050 (1974).

[4] BRAGINSKII, S. I., Reviews of Plasma Physics, Vol. 1, p. 205 (ed. by Leontovich, M. A.) Consultants Bureau, New York (1966).

[5] KIMURA, H., MAEDA, H., UEDA, N., SEKI, M., KAWAMURA, H., et al., Nucl. Fusion 18 (1978) 1195.

[6] MAHDAVI, M. A., DeBOO, J. C., HSIEH, C. L., OHYABU, N., STAMBAUGH, R. D., and WESLEY, J. C., Phys. Rev. Lett. 47 (1981) 1602. In this paper, the radiation power in the divertor is not explicitly taken into account in the discussion of the scrape-off plasma characteristics. However, a 1-D simulation similar to the one described in §6.5 shows that T_b is well approximated by $\left(\frac{7}{2}\frac{Q_b}{K_o}\ell\right)^{\frac{2}{7}}$ even in a strong radiation case.

[7] NAGAMI, M., MAEDA, H., KASAI, S., YAMAUCHI, T., SENGOKU, S. et al., J. Nucl. Mat. 76 & 77 (1978) 521.

[8] OHYABU, N., DEBOO, J. C., GROEBNER, R. J., MAHDAVI, M. A., TAYLOR, T., and WESLEY, J.C. "Effect of Divertor Geometry on Impurity Exhaust" Report No. GA-A16355, 1981 (unpublished).

7. Summary of Conclusions

Divertor actions on impurity removal, helium ash compression and radiative cooling have been studied in Doublet-III with an emphasis on the applicability to INTOR-like devices. The following principal results have been obtained with a single-null poloidal divertor where no divertor-chamber or divertor throat exists (referred to as "open divertor geometry") and the divertor coils are located outside the vacuum chamber.

1) As for reduction of impurities with an open divertor geometry :

Metallic impurities are reduced by a factor of 5 - 10 by a divertor. A factor of ~ 10 reduction is seen in carbon influx. Oxygen is reduced only modestly, but a factor of two reduction is observed in the radiation loss, and a typically peaked radiation power profile is changed into a hollow profile by a divertor.

2) As for demonstration of helium ash exhaust capability :

In helium-seeded divertor discharges, helium gas pressure near the divertor is observed to increase with the increase of the main plasma density. The maximum observed helium pressure is 1×10^{-4} Torr. The helium concentration in the main discharge is deduced to be ~1.6 % from the increase of electron density with the helium gas-puff. This pressure value is high enough to demonstrate the possibility of helium ash exhaust in a diverted tokamak like INTOR with practical-sized pumping ducts.

3) As for reduction of the heat load of the divertor plates by remote radiative cooling :

a) The radiation power in the divertor volume significantly increases with the increasing plasma density in the main plasma. The maximum observed radiation power is as much as 50 % of the ohmic input power. The radiation power in the main plasma is approximately constant (20 - 30 % of the ohmic input power). This remote radiative cooling has reduced the heat load of the divertor plate. The electron temperature near the divertor plate is cooled down to several eV. A significant increase is also observed in the divertor plasma density (higher than 5×10^{13} cm^{-3}). A simple one-dimensional numerical simulation of the radiative divertor elucidates the role of remote radiative cooling in the formation of dense and cold divertor plasma. This remote radiative cooling scheme has the advantage of cooling the divertor plasma without cooling the edge of the main plasma. If this edge cooling scheme can be applied to a diverted tokamak reactor, it may possibly reduce the heat load and the erosion problems of the divertor plates, which are the major drawbacks of a diverted tokamak reactor.

b) The source of this remote radiative cooling power is experimentally determined to be a mixture of line radiation of hydrogen neutral and oxygen. A simple model calculation of impurity line radiation in the divertor shows the feasibility of the remote radiative cooling in INTOR-like large-scale devices.

In light of obtaining these useful results, the installation of a divertor in reacting-plasma-grade fusion devices appears to be very effective for sustaining the long-lived operational conditions of a reacting plasma.

4) Subjects for future investigation

The ultimate goal of the divertor studies in Doublet-III is to provide physics design basis of the diverted tokamak reactors, like INTOR. With ohmically-heated diverted discharges in Doublet-III,

1) impurity reduction with open geometry,

2) helium ash compression,

3) remote radiative cooling (heat load reduction of the divertor plates) have been investigated and have culminated in this dissertation. These three subjects are key issues of divertor studies, and should be investigated further with beam-heated discharges, to demonstrate these three key aspects with conditions in close proximity to the fusion reactors.

In order to investigate the divertor physics in detail, the author proposes the following diagnostics that directly measure important physical quantities.

a) scanning Langmuir probe (n_e, T_e and particle flux)

b) Langmuir probes on the surface of the divertor plate

c) vuv spectrometer (line radiation, impurity concentration)

d) visible doppler spectrometer (ion temperature and neutral energy)

The divertor simulation codes that deals with processes of particle ionization, particle recycling, charge-exchange, line radiation, and electrostatic field should be developed to understand the divertor physics by comparing the calculated and experimentally obtained quantities.

Acknowledgements

The author wishes to express his sincere appreciation to Drs. Shigeru Mori, Yasuo Iso, Ken Tomabechi, Yukio Obata, Masaji Yoshikawa and Noboru Fujisawa at the Japan Atomic Energy Research Institute as well as to Dr. Tihiro Ohkawa at the General Atomic Company (San Diego, California, U.S.A.) for their continuing support and encouragement.

The author would like to express special appreciation to Dr. Masayuki Nagami and Dr. Akio Kitsunezaki for their excellent guidance throughout this work. Special thanks are due to Drs. Yasuo Shimomura, and Shigeru Konoshima for much constructive criticism. Collaboration and coorperation by Dr. Chung Liu Hsieh in bolometer array, Drs. Kimihiro Ioki and Masaki Maeno in limiter calorimetry, Drs. Neil. H. Brooks, Richard J. Groebner and Shigeru Izumi in spectroscopy, and Dr. John S. deGrassie in neutral pressure measurements was indispensable in this work. The author also wishes to thank Drs. Hideaki Yokomizo, Kichiro Shinya, and Hidetoshi Yoshida for their collaboration and stimulating discussions. The communication of experimental results on helium enrichment from the General Atomic Expanded Boundary Group was extremely valuable. The author wishes to thank Drs. James C. deBoo of GAC and Toshio Hirayama of JAERI for valuable imformation on the neutral helium measurement. He also wishes to thank Dr. Tomonori Takizuka of JAERI, Dr. Masana Nishikawa of Mitsubishi Atomic Power Industries, Inc., Drs. Dave Overskei and Keith H. Burrell of GAC and Dr. Doug E. Post of PPPL for fruitful discussions. This experiment was carried out with the fine support of the Doublet-III diagnostics group under Dr. R. Fisher and the machine operations group under

Dr. R. Callis. The author would like to express full gratitude to Dr. R. Hulse of the Princeton Plasma Physics Laboratory, Princeton, New Jersey for supplying us with a multi-species impurity code.

Finally, the author wishes to express his deep thanks to Professor Tadashi Sekiguchi of the University of Tokyo for his continuing encouragement and advice during the preparation of this manuscript.

Publication list in direct connection with this dissertation

[1] NAGAMI, M., SHIMADA, M., YOKOMIZO, H., SEKI, S., KONOSHIMA, S., et al., Nucl. Fusion 20 (1980) 1325. (Chapter 3, 4)

[2] NAGAMI, M., FUJISAWA, N., IOKI, K., KITSUNEZAKI, A., KONOSHIMA, S., et al., in Plasma Physics and Controlled Nuclear Fusion Research (Proc. 8th Int. Conf. Brussels, 1980) Vol. 2, IAEA, Vienna (1981) 367. (Chapter 3, 4)

[3] SHIMADA, M., IOKI, K., NAGAMI, M., YOKOMIZO, H., IZUMI, S., et al., in Controlled Fusion and Plasma Physics (Proc. 10th Europ. Conf. Moscow, 1981) Vol. 1 (1981) J1. (Chapter 4, 5, 6)

[4] SHIMADA, M., NAGAMI, M., IOKI, K., IZUMI, S., MAENO, M. et al., Phys. Rev. Lett. 47 (1981) 796. (Chapter 5, 6)

[5] SHIMADA, M., NAGAMI, M., IOKI, K., IZUMI, S., MAENO, M. et al., Nucl. Fusion 22 (1982) 643. (Chapter 4, 6)

[6] SHIMADA, M., NAGAMI, M., IOKI, K., IZUMI, S., MAENO, M., et al., "High Density, Single-Null Poloidal Divertor Results in Doublet III", to be published in J. of Nucl. Mat. (Chapter 4, 5, 6).

APPENDIX 1

Calculation of Non-coronal Radiative Cooling Rate of Oxygen

The radiative cooling rate by oxygen is calculated as follows. The rate equations are:

$$- n_e n_j S_j + n_e n_{j-1} S_{j-1} - n_e n_j \alpha_j + n_e n_{j+1} \alpha_{j+1} - \frac{n_j}{\tau} = 0$$

(j = II, III ... VIII)

$$n_e n_{VIII} S_{VIII} - n_e n_{IX} \alpha_{IX} - \frac{n_{IX}}{\tau} = 0$$

$$\sum_{j=I}^{IX} n_j = n_{ox}$$

where subscript j : ionization stage (j = II means + 1 ion),

n_e : electron density,

n_j : oxygen particle density in the ionization stage j,

S_j : ionization rate from j ion to (j+1) ion,

α_j : recombination rate from j ion to (j-1) ion (sum of radiative recombination and dielectronic recombination),

τ : recycling time (assumed to be the same for all ions),

n_{ox} : total oxygen density.

With Te, n_e, τ given, the fraction of each ionization stage f_j (= n_j/n_{ox}) is calculated, and the total radiative cooling rate L is given by:

$$L = \sum_{j=1}^{IX} f_j L_j \quad \left(= \frac{P}{n_e n_{ox}} \right)$$

where L_j is the radiative cooling rate for ions in the ionizaiton stage j (sum of excitation loss, ionization loss, and recombination loss), P is the total radiative power of oxygen. The ionization, recombination, and radiative cooling rates are calculated by a multi-ion species code [1]. The calculated L is shown in Fig. A-1. L is calculated for $n_e = 1 \times 10^{14}$ cm^{-3}, 2eV < T_e < 1 keV, τ = 0.1 ms, 1 ms, ∞ (coronal equilibrium). The coronal equilibrium calculation by Tarter [2] is also shown in the figure.

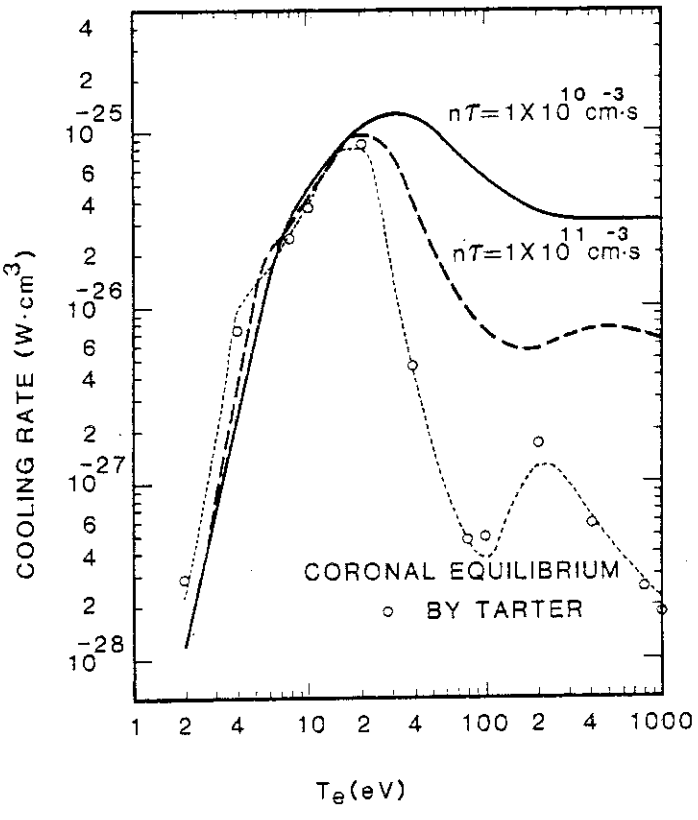

FIG. A-1 Non-coronal radiative cooling rate of oxygen.

REFERENCES (Appendix)

[1] HULSE, R., private communication. The atomic physics used in this code is the same as is described in POST, D. E., JENSEN, R. V., TARTER, C. B., GRASBERGER, W. H., and LOKKE, W. A., Atomic Data and Nuclear Data Tables 20 (1977) 397.

[2] TARTER, C.B., J. Quant. Spectrosc. Radiat. Transfer 17 (1977) 531.